p53 mediated regulation of LINE1 retrotransposition derived R-loops

Pratyashaa Paul[1], Arun Kumar[1], Astik Kumar De[1], Ankita Subhadarsani Parida,[1] Gauri Bhadke[1], Satyajeet Khatua[1], Fizalin Pattanayak[1], Bhavana Tiwari[1#]

[1]Department of Biological Sciences, Indian Institute of Science Education and Research Berhampur, India

[#]Correspondence: btiwari@iiserbpr.ac.in

Bhavana Tiwari, PhD
Intermediate Fellow, DBT-Wellcome Trust India Alliance
Department of Biological Sciences,
Indian Institute of Science Education and Research Berhampur,
Berhampur, Odisha 760010, India

Abstract

Long Interspersed Nuclear Element 1 (LINE1/L1) retrotransposons, comprising around 17% of the human genome, typically remain quiescent in healthy somatic cells but become activated in various cancer types. Our recent investigation reveals that p53 silences L1 transposons in human somatic cells, potentially constituting a tumor suppressive pathway. In this study, we demonstrate that p53 silences both L1mRNA-gDNA (cis L1 R-loops) and L1mRNA-cDNA hybrids (trans L1 R-loops) formed during retrotransposition. The activation of L1 transposons by HDAC inhibitors (HDACi) led to accumulation of these cis and trans L1 R-loops in p53$^{-/-}$ cells, which were mitigated by treatment with a reverse transcriptase inhibitor. Furthermore, p53 established re-silencing of hyperactivated L1 transposons induced by HDACi. The p53-mediated restoration of silencing was accompanied by recruiting histone repressive marks specifically H3K9me3 and H3K27me3 and inhibiting the deposition of H3K4me3 and H3K9ac marks at the L1 promoter. This study elucidates a novel role of p53 in regulating the formation of RNA-DNA hybrids, a pivotal intermediate component of retrotransposition, and initiating the suppression of hyperactivated L1 elements. These findings underscore the significance of p53 in preserving genome stability through the regulation of L1-derived R-loops.

In Brief: The role of L1 transposon derived L1mRNA-cDNA hybrids; an intermediate product formed during retrotransposition, in DNA damage and inflammation is not clear. Paul et al. reveals that p53 prevents L1cDNA derived RNA-DNA hybrids to control DNA damage and activation of inflammatory genes. The findings also elucidate the role of p53 in initiating the repression of hyperactivated transposons by facilitating the recruitment of epigenetic repressive marks and preventing the deposition of activating marks at L1-5'UTR.

"**Keywords:** p53, L1/LINE1, R-loops, RNA-DNA hybrids, Cis R-loop, Trans R-loop, Transposons, HDAC inhibitors

<u>Highlights</u>

1. p53 loss facilitates accumulation of both cis (L1mRNA-gDNA) and trans (L1mRNA-cDNA) forms of L1 R-loops.
2. The youngest, actively retrotransposing full-length L1s contribute to the formation of trans (L1mRNA-cDNA) R-loops.
3. p53 aids immediate L1 re-silencing by restoring deposition of epigenetic repressive and inhibition of activating marks.

4. Reverse transcriptase inhibitor prevents L1 mediated DNA damage.

Subject Categories: L1/LINE1, p53, Retrotransposons, RNA-DNA hybrids, Cis R loops, Trans R-loop, L1/LINE1

Introduction

p53 is the most commonly mutated tumour suppressor gene [1] and activates its downstream effectors to regulate cell cycle, apoptosis and senescence pathways to maintain genome integrity [2]. Recent studies have shown that p53 represses mobile genetic elements, suggesting a new axis of tumor suppression [3-6]. p53 mediated retroelement repression is conserved across various species, including flies, fish, and human somatic cell lines [7-10]. Employing CRISPR-mediated wild-type (wt) and p53 knockout ($p53^{-/-}$) cells, we have identified p53 binding motifs within the 5'UTR of L1 retrotransposons, and work from others predicted in Alu sequences [11-13]. By utilizing the synthetic L1-5'UTR-eGFP reporter, we demonstrated that p53 maintains repression of L1 within human somatic cell lines by facilitating the deposition of epigenetic repressive marks at the 5'UTR promoter to exert its repressive function [9]. Several other studies have underscored a direct correlation between increased retroelement expression and p53 mutations within cancer contexts [5,14,15]. These collective observations prompted an exploration into the potential involvement of p53 in initiating the silencing of activated L1 transposons and delineating the underlying mechanisms of *de novo* silencing. To address this, we employed HDAC inhibitors Trichostatin (TSA) and Sodium Butyrate (NaB) drugs that are known to induce repetitive elements, including L1 transposons on wt and $p53^{-/-}$ cells [16-18]. We examined the role of p53 in L1 resilencing function, a process that mirrors the epigenetic reprogramming observed in early embryos and primordial germ cells *in vivo*.

The initiation of L1 retrotransposition process involves transcription followed by the translation of two essential L1-encoded open reading frame proteins (ORFps); ORF1p and ORF2p. The combined efforts of ORF1p and ORF2p facilitate L1 retrotransposition and are linked to various diseases [19-23]. These proteins are crucial for the reverse transcription of L1cDNA and its subsequent integration. During mobilization, these ORFs are transcribed by RNA pol II, leading to the formation of a L1mRNA-gDNA hybrid as a transcriptional intermediate, if these structures persists can lead to the formation of 'cis R-loops'. R-loops represent three-stranded nucleic acid structures composed of an RNA/DNA hybrid alongside a displaced single-stranded DNA (ssDNA) and these can lead to either physiological or pathological outcomes. L1 encoded ORF2 protein contains two functional domains essential for target-primed reverse transcription: the Endonuclease (EN) domain creates a single-stranded DNA nick for integration, and the Reverse Transcriptase (RT) domain primes

complementary DNA synthesis based on the L1mRNA template. The recent structural findings on ORF2p identified domains that show extensive interactions with RNA templates [24]. The reverse transcription function of ORF2p generates a L1mRNA-cDNA hybrid structure, hence referred to as 'trans R-loop' intermediate structure comprising a free and un-nicked DNA segment, a nicked DNA, the newly synthesized cDNA, and L1mRNA serving as the template for reverse transcription, probably the four stranded non-canonical form of R-loops. L1 derived cDNA acts as triggers for type 1 interferon response, leading to the formation of inflammasomes [25]. Ectopic accumulation of (cis) R loops, particularly those arising from transcriptional events, is associated with various genomic and epigenetic instabilities [26-28]. These R-loops are implicated in genome instability [29] and DNA damage through several mechanisms: initiating abnormal replication [30], inducing transcription stress, and facilitating collisions between transcription and replication processes [26]. Consequently, the accumulation of cis and trans R-loops derived from L1 sequences can potentially lead to DNA damage and inflammation, an aspect of L1 pathogenesis that remains unexplored. L1-derived RNA/DNA hybrids may be exported to the cytosol via an as yet unidentified process, where they are detected by sensors such as endosomal TLR3 and the membrane-bound cGAS inflammatory pathway [31]. The L1 retroelement has the capability to retrotranspose Alus [32,33] and SVAs [34,35] hence these elements can also participate in the generation of unscheduled R-loops in the genome. There have been reports of ~100 L1-mediated insertions, the end product of retrotransposition, leading to genetic diseases. These retroelement insertions have been linked to the transmission of congenital disorders through the germ line, familial predispositions to cancer, as well as other conditions like β-thalassemias, and hemophilias [36-38]. However, there is an increasing acknowledgment that active L1s in somatic tissues also present inherent oncogenic hazard [3,5,15].

Herein, we establish the role of p53 in controlling the intermediate components of L1, retrotransposition specifically L1mRNA-cDNA hybrids, referred to here as 'L1 trans R-loops', formed during reverse transcription, and its role in genome instability. We present evidence indicating that the most recently evolved full-length retrotransposition-competent L1 elements are actively involved in the generation of trans R-loops. This assertion is supported by our analysis of DRIP-seq (DNA-RNA immunoprecipitation sequencing) data, along with validation conducted through DRIP-qCR (quantitative PCR) experiments. Furthermore, our findings reveal that the over-expression of the RT domain of L1-ORF2p led to a notable increase in trans R-loop accumulation, which was accompanied by heightened levels of DNA damage and inflammation. Interestingly, treatment with a reverse transcriptase inhibitor attenuated these elevations in DNA damage and inflammation markers, underscoring the oncogenic implications of L1-derived trans R-loops. We also demonstrate that p53 mediates *de novo* silencing of hyperactivated L1 retroelements employing HDAC inhibitor

118 (HDACi) treated cancer cell lines. Using synthetic L1-5'UTR-eGFP wt and p53$^{-/-}$ reporters,
119 combining with HDACi exposure, we observed highly de repressed L1 transposons in both the
120 genotypes. However, upon the withdrawal of HDACi drugs, the silencing of de repressed L1
121 transposons and its retrotransposition intermediates was immediate in wt p53 cells but not in p53$^{-/-}$
122 cells. This restoration of L1 silencing in wt L1 reporter coincided with the recruitment of histone
123 repressive marks and the removal of activating marks at the L1-5'UTR providing insights into
124 potential therapeutic strategies for diseases associated with L1 activation.
125
126 **Results**
127 **p53 controls L1 retrotransposition intermediary components**
128 Recently, our research demonstrated that p53 plays a crucial role in suppressing L1 transposons at
129 the transcription levels in human cell lines under non-stress conditions [9]. Building upon these
130 findings, our current study delves into the consequences of p53 deficiency on the regulation of
131 intermediary by-products of L1 activity, specifically RNA-DNA hybrids formed during
132 retrotransposition. Here, we noted heightened levels of L1 transcripts (**Figures** 1A and B) and ORF1
133 protein (**Figures** 1C and 1D) in both p53$^{-/-}$ cell lines (A375 and U2OS) generated using CRISPR
134 cas9 methodology **(Figures** S1A and B**)**, consistent with our prior study [4]. The immunofluorescence
135 (IF) experiments in wt and p53$^{-/-}$ cells with s9.6, a widely used antibody to visualize and detect the
136 RNA-DNA hybrids of R-loops [39], showed an increased signal of cytoplasmic RNA-DNA hybrids in
137 p53$^{-/-}$ (**Figures** 1E and 1E') as compared to the parental wt cells. Next, DNA-RNA
138 immunoprecipitation (DRIP) assays were conducted utilizing the s9.6 antibody to investigate the
139 propensity of L1 element in the participation of R-loops in p53$^{-/-}$ cells (**Figure** 1F). In this experiment
140 s9.6 antibody was used to precipitate RNA-DNA hybrids structures followed by quantification by
141 qPCR using the primers that binds the DNA region of interest to measure the binding [40]. Mapping
142 experiments with DRIP-qPCR using primers spanning 5'UTR, ORF1, and ORF2 regions revealed
143 that the L1-5'UTR region, which harbors RNA pol II promoter, was predominantly enriched in R-
144 loops derived RNA-DNA hybrids, whereas the ORF2 region exhibited a modest enrichment. The
145 specificity of our assay for detecting RNA-DNA hybrids was validated by pre-treating the samples
146 with RNase H before the antibody pulldown (data not shown), resulting in the complete abolition of
147 our ability to amplify the region. Given that the majority of the nuclear R-loop derived RNA-DNA
148 hybrids was observed in the cytoplasm, we leveraged an alternative method to specifically probe R-
149 loops. This involved the overexpression of RNaseH1 with D210N catalytic dead mutant (RNH-GFP)
150 with the nuclear localization signal fused at the N-terminus in A375 wt and p53$^{-/-}$ cells [27,40,41]. Stable
151 cell lines of RNH-GFP showed the similar GFP expression between these genotypes. qPCR

experiments from GFP immunoprecipitated samples indicated stronger R-loop signal at L1-5'UTR and a weaker signal at the gene body L1-ORF2 in RNH-GFP cells, similar to s9.6 pull down data **(Figures** 1G and 1H**)**. Moreover, our analysis of DRIP-seq and Global Run-On sequencing (GRO-seq) data unveils a partial overlap of peaks between RNA-DNA hybrid sequences and nascent transcripts at the L1-5'UTR coordinates (cis R-loops). Conversely, no overlapping peaks were observed at the L1-ORF2 region in these two sequencing datasets (**Figure** 1I), suggesting that 5'UTR region demonstrates a higher tendency to form cis R-loops, likely due to nascent RNA annealing. Conversely, ORF2 region possibly be involved in generation of trans R-loops, originating from distant L1mRNAs.

p53 prevents the formation of L1 trans R-loop derived RNA-DNA hybrids

During the retrotransposition life cycle, the full-length L1 undergoes a process in which it generates an identical DNA copy of itself, known as L1cDNA, through the reverse transcription of L1mRNA. Hence, within the retrotransposition life cycle, there is potential for the formation of two types of RNA-DNA hybrids that can serve as R-loop; cis R-loops (L1mRNA-gDNA) occurring at the L1 5'-UTR promoter level during transcription, and trans R-loops (L1mRNA-cDNA) formed during reverse transcription. Genome-wide DRIP-seq studies reveal that cis R-loops are predominantly found in GC-rich regions and promoters [42,43]. The recent findings demonstrate that p53 plays a role in global regulation of cis R-loops and viral proteins induce R-loops in p53 inhibited cells [44,45]. However, the precise mechanism by which p53 regulates L1 derived R-loops has yet to be explored. The analyses of DRIPseq data from IMR-90, HEK293T, and k562 cell lines known to harbour p53 mutations (PMID: 26579211) revealed that young L1 subfamilies, which are capable of retrotransposition, participate in R-loop formation **(Figure** 2A**)**. Further, to investigate whether L1 hyperactivation leads to increased accumulation of R loop formation, we treated A375 wt and p53$^{-/-}$ cells with an HDAC inhibitor Sodium Butyrate (NaB) **(Figure** 2B**).** RNAseq analyses on NaB (PMID: 38410440, 38410440) and TSA (PMID: 37496675) exposed cells and qRT-PCR on NaB treated A375 wt and p53$^{-/-}$ did, in fact, show that L1 expression was elevated upon HDAC inhibition (**Figures** 2B and C). IF assays on wt and p53$^{-/-}$ cells treated with NaB revealed an increased signal of s9.6 detecting the RNA-DNA hybrids **(Figures** 2D-2E'**)**. Significantly, rescue experiments employing 3TC, a well-known reverse transcriptase inhibitor that inhibits L1cDNA formation, led to decreased s9.6 signals in both NaB-treated wild-type (wt) and p53$^{-/-}$ cells. This implicates that L1 reverse transcription is involved in generating L1 R-loops (L1mRNA-cDNA) derived RNA-DNA hybrids (**Figures** 2E and E'). Subsequent qRT-PCR analysis of RNA-DNA hybrids precipitated by s9.6 antibodies from A375 wt and p53$^{-/-}$cells, upon 3TC treatment, demonstrated complete depletion of R-loops from the L1-ORF2

186 region, with a modest reduction observed at the 5'-UTR (**Figure** 2F). This verifies the likelihood of
187 L1-ORF2 being prone to trans R-loop formation. Similar outcomes were obtained via
188 immunoprecipitation using a GFP antibody from cells expressing RNH-GFP (**Figure** 2G). These
189 findings underscore that although the majority of the L1 5'-UTR region contributes to cis R-loop
190 formation, L1-ORF2 likely facilitates trans R-loop formation, highlighting the involvement of L1 in
191 both types of R-loop signals, arising from L1mRNA-gDNA as well as L1mRNA-cDNA hybrids.
192 Next, we conducted overexpression of L1-encoded proteins- ORF1p, EN and RT enzymatic
193 domains of ORF2p c-terminally fused with GFP and empty vector (EV) as a negative control, in $p53^{-}$
194 $^{/-}$ cells of A375 and U2OS cell to investigate the potential impact of these overexpressed proteins on
195 the abundance of RNA-DNA hybrids. It has been established that the RT domain maintains reverse
196 transcriptase activity autonomously within the cytoplasm [24]. Overexpression of RT domain resulted
197 in elevated levels of cytoplasmic RNA-DNA hybrids, consistent with recent findings reported by
198 Kathleen's group [24], as evidenced by increased s9.6 signals in the IF experiments **(Figure** 3A**)**. This
199 was accompanied by elevated transcript levels of DNA damage indicators (RAD51, BRCA1, and Rb)
200 and inflammatory gene markers (IL6, STING pathway, IRF-7, MCP-1, CXCL-10, IFN-β, and ISG-15)
201 measured using the qRT-PCR experiments **(Figure** 3B**)**. Upon 3TC treatment, the augmented RNA-
202 DNA hybrids in $p53^{-/-}$ overexpressing ORF1p-GFP, EN-GFP, and RT-GFP were mitigated **(Figure**
203 3A'**),** confirming the involvement of L1cDNA derived RNA-DNA hybrid formation. This was
204 corroborated by decrease in accumulation of RAD51, BRCA1, RB and inflammatory gene markers
205 **(Figure** 3B**)** suggesting the aberrant formation of L1mRNA-cDNA with deleterious effects on genome
206 stability. Moreover, to confirm if the overexpression of the RT-GFP leads to the generation of L1
207 trans R-loops, we conducted sequential DRIP-qPCR experiments (**Figure** 3C). These experiments
208 involved immunoprecipitation using GFP from *in vivo* RNH-GFP expressing $p53^{-/-}$ followed by IP with
209 s9.6 antibodies to capture R-loops. This sequential immunoprecipitation assays validated that RT
210 domain alone can specifically facilitate formation of R-loops in $p53^{-/-}$. Following this, IF assays
211 utilizing the yH2AX antibody demonstrated increased DNA damage in cells with overexpression of
212 the RT domain **(Figures** 3D and D'**)** suggesting that RT domain alone is capable of inducing L1cDNA
213 potentially culminating in the formation of L1trans R-loops derived RNA-DNA hybrids and
214 subsequent DNA damage.
215
216 **p53 promotes establishment of L1 re-silencing**
217 Given our findings that delineate trans-repressive functions of p53 in maintaining repression of L1
218 RNA-DNA hybrids, we sought to investigate its potential role in mediating the re-establishment of L1
219 silencing. To assess this, we employed HDACi drugs; TSA and NaB to induce L1 activation in a

220 reporter system where 5'UTR-eGFP of L1 retrotransposons is inserted at the huAAVS1 site in both
221 p53 wt and p53$^{-/-}$ cells of U2OS **(Figures** 4A-F**)** and A375 **(Figures** S2A-G**)** [5]. Following a 24-hour
222 treatment with HDACi drug (Figure 4A), activation of L1 reporters were assessed by quantifying the
223 GFP positive cells by comparing the DMSO and 24 h TSA panels using the confocal microscopy.
224 The efficacy of both wt and p53$^{-/-}$ cells to suppress L1-5'UTR-eGFP upon drug withdrawal of 3 and
225 6 days elucidated a complete silencing of GFP in wt but not in p53$^{-/-}$cells, this can be observed by
226 comparing the panels of cells treated with DMSO and those observed at 4 and 7 days **(Figure** 4B**).**
227 Similarly, the expression levels of egfp transcripts correlated with increased GFP intensities in L1-
228 5'UTR reporter cells in response to HDACi **(Figures** 4C and 4D**)**. This activation of GFP closely
229 corresponded to activation of endogenous L1-ORF1, as demonstrated through RNA *in situ*
230 hybridization using stellaris probes **(Supplementary Table 2 for probe sequences) (Figure** 4B**).**
231 Four days after the withdrawal of TSA, the activity of the L1-5'UTR reporter returned to uninduced
232 levels in p53 wt cells, but not in p53$^{-/-}$. No variation was detected in cellular proliferation using the
233 cell glow titre test between wt and p53$^{-/-}$ A375 L1-5'UTR-eGFP reporters following HDACi treatment
234 **(Figure** S2A**)**. Similarly, using qRT-PCR and microscopy, the reactivation of GFP and L1-ORF1 and
235 subsequent re-silencing were also detected in A375 wt after 24 treatment with HDAC inhibitors
236 followed by 4 days of withdrawal, but not in the p53$^{-/-}$ cells **(Figures** S2B-E**)**. In line with previous
237 research on HDACi treated embryonic stem cells [16], our experimental model demonstrated that
238 inhibiting HDAC with TSA led to hyperacetylation of histones H3 and H4. This was evident from the
239 increased signal observed in western blotting when probed with antibodies targeting H3Ac and H4Ac
240 in both U2OS L1-5'UTR **(Figures** 4E and 4F**)** and A375 L1-5'UTR reporter cell lines **(Figures** S2F
241 and S2G**)**.
242 Next to determine whether p53 also enables resilencing of retrotransposition activation, we
243 used a synthetic L1 designated 99-gfp-LRE3 retrotransposition indicator [46,47], using HDACi
244 treatment, similar experiment was conducted on stably transfected parental wt and p53$^{-/-}$ U2OS cells,
245 schematic shown (**Figure** 6A). This indicator **Figure** 6B mimics retrotransposition cycle generating
246 all L1 intermediate components allowing direct measurements of *de novo* retrotransposition rates by
247 visualising GFP positive cells (green cells). Consistent with the L1-5'UTR reporter, we noted re-
248 silencing of L1-retrotransposition in wt cells upon withdrawal experiments after TSA and NaB
249 treatments. Whereas no re-silencing was observed in p53$^{-/-}$ cells as quantified in **(Figures** 6C- 6D'**)**.
250
251 **p53 promotes restoration of deposition of histone repressive marks at L1-5'UTR**
252 In a previous study, we demonstrated that p53 regulates L1 transposons by epigenetic mechanisms
253 [9]. To investigate whether p53 can facilitate re-silencing of L1 by recruiting these marks, we activated

254 L1 transposons in both A375 wt and p53$^{-/-}$ L1-5'UTR-eGFP reporters, as demonstrated in **Figure 6**.
255 The quantification of histone repressive marks H3K9me3 and H3K27me3 was performed with ChIP-
256 qPCR studies using primer sets targeting the p53 binding site at the L1-5'UTR (**Figure** 6A). Upon
257 treatment of cells with HDACi drug (NaB), L1 activation coincided with depletion of H3K9me3 **(Figure**
258 6B**)** and H3K27me3 **(Figure** 6C**)**, as well as acquisition of H3K9Ac **(Figures** 6D**)** and H3K4me3
259 **(Figures** 6E**).** Further, levels of H3K9 and H3K27 trimethylation reversed back to the DMSO treated
260 levels following a 4-day drug withdrawal experiment in wt cells with a concurrent decrease in H3K9Ac
261 marks and H3K4me3. Notably, changes were not observed in p53$^{-/-}$ cells. Importantly, this alteration
262 in chromatin marks closely correlated with the reversal of L1 induction observed in wt cells, providing
263 the evidence that p53 initiates the re-silencing of activated L1 transposons by promoting the
264 recruitment of epigenetic repressive marks and removal of activating marks **(Figures** 4, 6 and S2**)**.
265
266 **A LINE1 reverse transcriptase antagonist partially reverses DNA damage triggered by L1**
267 The findings depicted in **Figures** 4 and S2 demonstrate that p53 establishes resilencing of L1-
268 transposons upon HDACi withdrawal by mediating recruitment of epigenetic repressive and inhibiting
269 activating marks at L1-5'UTR. HDACi is shown to induce DNA double-strand breaks in cancer cells
270 [48]. Therefore, to investigate the involvement of p53 in the reversal of L1 retroelement-induced DNA
271 damage, we subjected U2OS wt and p53$^{-/-}$ cells to HDACi (**as shown in Figure** 7A) (**as shown in**
272 **Figure** S3), followed by exposure to either DMSO or 3TC. Previous study from us has shown L1-
273 mediated genomic rearrangement in early passages of p53$^{-/-}$ cells [4], and similarly, we observed
274 induction of L1-ORF1p de repression accompanied by DNA damage upon TSA treatment in both
275 the wt and p53$^{-/-}$ U2OS cells. The treatment of p53$^{-/-}$ cells with 3TC resulted in restoration of L1-
276 ORF1p expression to the vehicle (DMSO) treated level, accompanied by a notable decrease in the
277 number of 53BP-1 foci, which serve as an indicator of DNA damage **(Figure** 7A**)**. Repair of DNA
278 damage and suppression of inflammatory genes to their uninduced levels occurred promptly in wt
279 cells, while it was impaired in p53$^{-/-}$ cells. Similar results were observed in staining with γH2AX, an
280 additional marker of double-stranded DNA breaks. **(Supplemental Figure** S3 A and A'**)**. Collectively,
281 our findings suggest that p53 facilitates the suppression of activated L1 transposons that trigger DNA
282 damage and inflammation. The immunofluorescence experiments on cells treated with DMSO and
283 NaB to evaluate the impact of HDACi on the acetylation and methylation levels of H3K9 and H3K27
284 histones in both wt and p53$^{-/-}$ cells detected a global increase in the acetylation of lysine residues on
285 the H3 protein, notably at positions 9 and 27, accompanied by a reduction in methylation at the same
286 lysine residues **(Figures** S4 and S5**)**. Administering 3TC for 4 and 7 days led to the re-establishment
287 of these histone marks in wt cells, but not in cells lacking the p53 gene.

288

289 **Discussion**

290 Our comprehensive analyses, combining experimental and bioinformatic approaches, unveil the
291 pivotal function of p53 in repressing RNA-DNA hybrids originating from L1 retrotransposition derived
292 R-loops encompassing both the cis (L1mRNA-gDNA) and trans (L1mRNA-cDNA) configurations
293 **(see Figures** 1 and 2**)**. While previous studies primarily focused on the mutagenic potential of L1 *de*
294 *novo* insertions, our understanding of the impact of nucleic acid intermediates like L1 RNA-DNA
295 hybrids and protein products such as L1-ORF1p and ORF2p in genomic instability and inflammation
296 remains limited. Despite the relatively infrequent detection of new L1 insertions in cancer genomes
297 compared to their deleterious activity, L1 activation is a common feature in many sporadic cancer
298 genomes, as evidenced by recent pan-cancer studies [25,49,50]. Our finding regarding the prominent
299 involvement of L1 promoter in cis R-loop formation aligns with previous genome-wide studies
300 highlighting the enrichment of R-loops in promoter regions globally [41]. This is corroborated by the
301 observation of overlapping peaks of DRIP-seq at the L1 promoter with those identified from the GRO-
302 seq, suggesting the occurrence of transcriptional pausing at L1-5'UTR that leads to the formation of
303 cis RNA-DNA hybrids. Conversely, the participation of L1-ORF2 genic region in trans R-loop
304 formation is validated by our observation of diminished R-loop signals upon 3TC treatment in RNH-
305 GFP expressing cells **(Figure** 3**)**. R-loops are capable of yielding both adverse and beneficial
306 physiological outcomes in a cell [51]. This prompted our speculation that R-loops originating from
307 retrotransposons could impede the finalization of insertions—a critical controlling step in the
308 retrotransposition process to prevent the amplification of L1 copies in the genome. However, the
309 observed decrease in DNA damage markers and inflammation upon RT overexpression, coupled
310 with a reduction in cytosolic RNA-DNA hybrids upon treatment with 3TC in DRIP-qPCR and
311 immunofluorescence assays, provides mechanistic insights into the contribution of RNA-DNA-
312 derived L1 R-loops to eliciting genome instability and inflammation, the two hallmarks of cancer. This
313 also indicates that, in addition to the canonical retrotransposition insertion, other intermediate
314 components can have oncogenic potential. These observations led us to speculate that L1 R-loops
315 may not only act as a bystander but as a double edged sword in this context.

316 Furthermore, the inhibition of HDACs resulted in the loss of methylation and the gain of
317 acetylation at the 5'UTR, activating L1 transposons and the derived R-loops (refer to **Figures** 3, 4,
318 5, and S2). Withdrawal of HDACi caused permanent L1 de repression in $p53^{-/-}$ cells, inducing DNA
319 damage and inflammation triggered by L1 R-loop-derived RNA-DNA hybrids. In contrast, wild-type
320 cells swiftly silenced L1 by promoting H3K9me3 and H3K27me3 (**Figures** 6 and 7). This mechanism
321 may confer cancer resistance in p53-driven cancers treated with HDACi [52]. Additionally, treatment

322 with 3TC prevented the activation of L1 RNA-DNA hybrids representing the first evidence of trans
323 L1 R-loop formation in p53$^{-/-}$ unstressed cells as well as in HDACi-treated cells.
324 Our findings also suggest that p53 promotes re-establishment of silencing of hyperactive L1s,
325 advancing our prior research underscoring the function of p53 in preserving L1 repression in human
326 somatic cell lines. Considering the function of p53 in mediating repression of L1s and L1-derived R-
327 loops, especially those originating from nuclear L1mRNA-cDNAs, these discoveries could hold
328 significant implications for elucidating the mechanisms underlying p53 tumor suppression. Unlike
329 conventional understandings, this study reveals that the RT domain is involved in regulating RNA-
330 DNA hybrids that triggers DNA damage as seen in **Figure 3**. These unexplored oncogenic risks
331 posed by the L1 RT domain trigger acute inflammatory transcriptional programs upon
332 overexpression, particularly in the absence of p53 [53-55]. Treatment with 3TC definitively prevented
333 the induction of nearly all inflammatory genes and DNA damage (**Figure 3)** in both wt and p53$^{-/-}$.
334 Since 3TC is a potent inhibitor of the L1 reverse transcriptase [56-58], these results indicate that L1
335 retrotransposition intermediates provoke inflammatory programms in p53 deficient cells.
336 Furthermore, these findings also suggest that the induction of immune response genes may stem
337 from the RT domain of ORF2p, attributed to the cytosolic accumulation of RNA-DNA hybrids, along
338 with the accumulation of trans L1 R-loops assessed in sequential DRIP-qPCR assays on RNH-GFP
339 *in vivo* system. Taken together, these findings suggest that incorporating a reverse transcriptase
340 inhibitor into personalized cancer therapy [59] could enhance the efficacy of HDAC inhibitor treatment
341 for cancer.
342
343 **Materials and Methods**
344 **Cell culturing:** p53 wild-type (wt) and p53 knockout (p53$^{-/-}$) cells of A375, U2OS cells were obtained
345 from Prof. John Abrams, UT Southwestern Medical Center, Dallas, Texas. A375 and U2OS cells
346 were cultured in Dulbecco's Modified Eagle's Medium (Gibco, #12100046). All cell lines were grown
347 at 37°C, 5% CO2 and passaged using Trypsin (Gibco, #15400054) in the presence of an anti-
348 antimycotic antibiotic (Gibco, #15240062) .
349
350 **Generation and screening of p53 knockout cells**
351 CRISPR cas9 editing (pX458), was used to generate p53$^{-/-}$ cell lines in the laboratory of Prof. John
352 Abrams at UTSW. p53$^{-/-}$ clones were identified by western blot using p53 monoclonal DO-1 (sc-
353 126) and L1-ORF1p expression levels were examined using anti L1-ORF1p antibody using
354 immunofluorescence experiments. Individual clones were grown until 100% confluent in 6-well plates
355 and whole cell lysates were prepared in RIPA lysis buffer (NaCl 140mM, EDTA 1uM, Tris HCl 10mM,

356 Triton X-100 1%, SDS 0.1%, Sodium Deoxycholate 0.1%) containing protease inhibitors (Roche).
357 Protein was quantified using Bradford assay (Protein Assay Kit, BioRad) and an equal amount of
358 total protein was loaded. Antibodies used were as follows: p53 monoclonal DO-1 (sc-126), anti L1-
359 ORF1p, clone4H1 (Millipore, #MABC1152) and β-actin (sigma, #A-2228). Sanger sequencing was
360 performed to confirm $p53^{-/-}$.
361
362 **Generation of huAAVS1 targeted L1-5'UTR-eGFP reporter cells**
363 The wt L1-5'UTR constructs, previously generated and kindly provided by Prof. John Abrams at
364 UTSW, were utilized. Stably transfected cells were created using huAAVS1-TALENL (Addgene
365 #59025) and huAAVS1-TALENR (Addgene #59026), along with donor plasmids. Three days after
366 transfection, single cells positive for GFP were sorted into 96-well plates using fluorescence-
367 activated cell sorting (FACS), following the protocol outlined in [4].
368
369 **For 3TC experiments**
370 2.5 x 10^5 wt and $p53^{-/-}$ A375 and U2OS cells were plated into 6-well plates. After overnight of seeding
371 media was changed with fresh media containing DMSO, HDACi. After 24 h of HDACi treatment
372 media was replaced with fresh containing 3TC (10 μM). After 4 days and 7 days of 3TC treatment,
373 cells were harvested for RNA isolation or analysed for microscopy. qRT-PCR was conducted using
374 Applied Biosciences QuantStudio 5. Gene expression was normalized to β-actin, and fold induction
375 was calculated relative to the wild type. Primer sequences utilized in this study are available in
376 **Supplemental Table 1**.
377
378 **Real Time PCR experiments (RT-PCR)**
379 Total RNA was isolated using TRIzol (Invitrogen), then treated with Turbo DNase (Thermo Fischer,
380 #AM1907) for removal of DNA. RT-PCR was conducted utilizing cDNA synthesis kit Verso (Thermo
381 Fischer, #AB1453A). Applied biosciences Quant studio 5 was used for real time PCR and
382 normalization of gene expression was done against β-actin (for standard gene expression analysis),
383 RPL134 for DRIP-qPCR experiments, and fold induction was determined relative to the wild type.
384 Refer to Supplemental Table 1 for the primer sequences employed in RT-PCR assays.
385
386 **Effect of HDACi in wt and p53 cells expressing LRE3 retrotransposition**
387 2.5 x10^5 cells were transfected with equal amounts of 99-GFP-LRE3 (LRE3) plasmid, as previously
388 described [34]. After 72 h, cells were selected for puromycin resistance. Similar protocol was
389 followed for HDACi exposure followed by 3TC as mentioned in **Figure** 4. Confocal imaging was

390 performed using LSM780 and LSM880 at the UTSW, Texas. GFP positive cells were counted from
391 5 images from each of the samples. 2 biological replicates were performed.
392 **Statistical Analysis**
393 Quantitative data were collected from experiments conducted in at least two or three biological
394 replicates with technical replicates. One tailed Student's t-tests were calculated from three biological
395 replicates to detect statistically significant differences (with a cutoff of *p<0.05 and **p<0.01).
396
397 **Drug treatment**
398 TSA (Sigma Aldrich, #T8552) and NaB (Sigma Aldrich, #567430) were purchased Sigma. All drug
399 treatments were carried out in DMEM (Gibco, #12100046) supplemented with 10% (vol/vol) FBS
400 (Gibco, #A5256701) and 100X anti-antimycotic (Gibco, #15240062). Treatment with TSA (100nM)
401 was for 24 hr as indicated in the figure legend. NaB was used at 25 μM as indicated.
402
403 **Cloning of NLS tagged RNaseH1 with D210N**
404 For NLS-tagged RNaseH1D210N, cDNA fragments (purchased from IDT) [60] containing human
405 RNaseH1 with D210N catalytic dead mutant was amplified by PCR for cloning in pEGFP-N1 using
406 EcoRI (NEB, #R3101S) and KpnI (NEB, #R3142S) restriction sites. One SV40 nuclear localization
407 signal (NLS) (CCCAAAAAGAAACGCAAAGTG) was introduced by forward primer at the PCR step.
408 Primers used in PCR amplification are listed in **Supplemental Table 1**.
409
410 **Generation of stable cell lines expressing RNaseH1 D210N (RNH-GFP)**
411 To study R-loop in wt and $p53^{-/-}$ cells, nucleus localization sequences containing GFP-tagged,
412 catalytically-inactive RNase H1 D210N was cloned in pEGFN-1. The cloned sequence was verified
413 by sanger sequencing and A375 wt and $p53^{-/-}$ cells were transfected for the stable cell line generation
414 using G418 (Gibco, #11811064).
415
416 **ChIP-qPCR**
417 One billion A375 wt and $p53^{-/-}$ cells were grown in a 150 cm^2 dish and were fixed with 1%
418 formaldehyde in flasks at room temperature for 10 minutes and subsequently washed with ice-cold
419 PBS before a 125mM glycine solution was added to stop the fixation. The cells were scraped from
420 the flask and were resuspended in ChIP lysis buffer (50 mM HEPES-KOH pH7.5, 140 mM NaCl, one
421 mM EDTA pH8, 1% Triton X-100, 0.1% Sodium Deoxycholate, 0.1% SDS, Protease inhibitor). The
422 cell lysate was sonicated using an M220 Focused-ultrasonicator (Covaris) to release chromatin
423 lengths to 400bp, peak power 75.0, Duty factor =10, cycles/Burst =200, for 240 seconds. Chromatin

424 was diluted ten times with RIPA buffer and incubated with the following antibodies – H3K9me3 (Cell
425 Signalling Technologies #13969), H3K27me3 (Cell Signalling Technologies, #9733), H3K9Ac (Cell
426 Signalling Technologies, #9649) . Parallel protein A/G beads (EMD Millipore, #IP0515ML), H3K4Me
427 (Cell Signalling Technologies, #9751) were charged and incubated with the antibodies overnight,
428 following high salt, low salt, and LiCl washes the next day and eluted. Eluted chromatin was treated
429 with RNAase A (Thermo Fischer, #12091021) and proteinase K (NEB, #P8107S), crosslinks were
430 reversed, and samples were purified using a PCR purification kit (Qiagen). ChIP enrichment was
431 quantified by qPCR with Quant Studio 5 (Applied Biosciences).
432
433 **DRIP-qPCR**
434 One billion A375 p53 wt and p53$^{-/-}$ cells or cells expressing RNH mutant were plated into a 150 cm^2
435 dish for overnight (Tarsons) and were fixed by 1% formaldehyde, followed by quenching via Glycine
436 to a final concentration of 125 mM. Cells were rinsed twice with 10 mL cold PBS. 5 mL of cold PBS
437 was added, dishes were scraped thoroughly with a cell scraper and transferred. Cells were lysed in
438 750 ul lysis buffer composed of 140 mM NaCl, 1 mM EDTA (pH8),1% Triton X-100, 0.1% Sodium
439 Deoxycholate,0.1% SDS, Protease Inhibitors (added fresh each time) per 10 million cells. Cell lysis
440 was performed at room temperature. The cell lysate was sonicated to shear DNA to an average
441 fragment size of 400 bp by the M220 Ultrasonicator (Covaris) as previously mentioned for
442 ChIP**.** Approximately 25 µg of RNA-DNA hybrid per IP was used. Each sample was diluted 1:10 with
443 RIPA Buffer (50 mM Tris-HCl, pH8,150 mM NaCl, two mM EDTA pH8, 1% NP-40, 0.5% Sodium
444 Deoxycholate, 0.1% SDS, Protease Inhibitors (added fresh each time). Primary antibody RNA-DNA
445 hybrid (s9.6) antibody (Merck Millipore, #MABE1095, 3ul) or GFP (Thermo Fisher, 5ul) was added
446 to all samples and incubated at 4°C for 2 h. 60 ul of Pierce A/G Agarose beads were taken for 25 ug
447 of RNA-DNA hybrid. Beads were charged and incubated with the antibody incubated sample at 4
448 degrees overnight in shaking. The immunoprecipitated samples were washed by low salt, high salt,
449 and LiCl wash buffers. RNA-DNA hybrids were eluted by slowly adding 120 µL of elution buffer (1%
450 SDS, 100mM NaHCO3) to the protein A/G beads and vortex for 15 min at 30°C. 4.8 µL of 5 M NaCl
451 and 2 µL RNase A (10 mg/mL) were added and incubated while shaking at 65°C overnight. 2 µL
452 proteinase K (20 mg/mL) was added and incubated while shaking at 60°C for one hour. The RNA-
453 DNA hybrids were purified using a PCR purification kit (QIAGEN). Analysis of RNA-DNA hybrid level
454 was performed by qPCR.
455
456 **Quantification of RNA-DNA hybrids.**

457 RNA-DNA Hybrid levels were measured by RT-PCR using 2X POWER UP SYBR Green (Invitrogen,
458 #A25741) and analyzed via the QuantStudio 5 Real-Time PCR System (Applied Biosciences).
459 Primer sequences are listed in **Supplemental Table S1**. The qPCR results were analysed using the
460 percentage input method. The RNA-DNA hybrid enrichment was calculated based on the IP/Input
461 ratio. Three biological replicates were performed. The result is the average of all the biological
462 replicates.
463
464 **Immunofluorescence**
465 A375 p53 wt and p53$^{-/-}$ cells were cultured on poly-L-lysine (Sigma, #P4707)-coated coverslips,
466 washed with PBS and fixed with 4% paraformaldehyde. The cells were treated with 0.1% Triton X-
467 100 in PBS and 10% fetal bovine serum and were subsequently incubated with primary antibodies
468 at room temperature for 1 hour or 4 degrees overnight. After washing, secondary antibodies were
469 added and incubated in the dark at room temperature for 1 hour. Cells were washed with PBS and
470 counterstained with DAPI before observation under an Apotome microscope (Zeiss). All images were
471 taken using the same microscope parameters, and fluorescence quantification was performed using
472 fiji J software. Primary antibodies used were LINE1 ORF1p (Merck Milipore, #MABC1152), Anti
473 RNA-DNA Hybrid antibody (Merck Milipore, #MABE1095), yH2AX (Invitrogen, #MA1-2022),
474 H3K9me3 (Cell Signaling Technologies, #13969), H3K27me3 (Cell Signaling Technologies, #9733),
475 H3K9Ac (Cell Signaling Technologies, #9649), and 53BP1 (Cell Signaling Technologies, #4937), all
476 at a dilution of 1:50. Secondary antibodies used were: anti-mouse 568 (Thermo Fischer, #A-11031),
477 anti-mouse 488 (Thermo Fischer,#A-10680), anti-rabbit 488 (Thermo Fischer, #A-11008), and anti-
478 rabbit 568 (Thermo Fisher, #A-11011), at a dilution of 1:1000.
479
480 **Microscopy**
481 Images were captured using 60x oil objective Zeiss LSM780, LSM880 (UT Southwestern Medical
482 Center, Dallas, Texas) and Leica sp8 (ILS Bhubaneswar BT/INF/22/SP28293/2018) confocal
483 microscope. Zeiss Apotome 3 fluorescent microscope (IISER Berhampur) was also instrumental for
484 imaging. All images were processed via Fiji software package.
485
486 **Cytotoxicity assay using cell glow titre assay**
487 A total of 5000 A375 wt-5'UTR and p53$^{-/-}$ -5'UTR cells were distributed evenly into 96 well plates,
488 with each well containing either DMSO or a solution of NaB or TSA followed by 3TC. The CellTiter-
489 GLO kit from Promega (G7570) was utilized. Cells were treated with HDACi for 24, 48 or 72 h. 25 ul
490 of CellTiter-Glo® Reagent was added and mixed thoroughly for 2 minutes using an orbital shaker.

491 The plate was kept at room temperature for 10 minutes and the luminous signals were quantified
492 using a plate reader after 24, 48 and 72 h of treatment as per the instructions. Results are quantified
493 in relation to the DMSO control for each genotype.
494
495 **RNA *in situ* hybridization assays**
496 LGC Biosearch Technologies' Stellaris® RNA FISH Probe Designer was used for the designing of
497 Qusar-568 probes for L1-ORF1 probes, for RNA *in situ* hybridization. Protocol was followed as per
498 the manufacturer's instructions.
499
500 **Dataset Analyses**
501 DRIP-seq data of various cell lines (PMID 26579211), were retrieved from the NCBI Gene
502 Expression Omnibus (GEO) in SRA format. Before analysis, the data underwent preprocessing to
503 remove adapters and low-quality bases. Subsequently, the cleaned reads were aligned to the
504 GRCh38 human reference genome assembly (hg38) using the STAR aligner (version 2.7.10a). To
505 identify regions enriched with potential R-loops, MACS3 (Model-based Analysis of ChIP-Seq)
506 (version 3.0.0) with the 'macs3 callpeak -t' option was employed, ensuring precise localization within
507 the genome. Additionally, RepeatMasker (version 4.1.6) was applied, utilizing the 'RepeatMasker -
508 engine rmblast' option, to mask retrotransposable elements and repetitive sequences, thereby
509 maintaining the integrity of subsequent analyses [61]. Expression levels of retrotransposable elements
510 were quantified from the alignment files generated by STAR, followed by normalization for library
511 size and transcript length. Heatmaps illustrating the expression patterns of retrotransposable
512 elements across different cell lines were generated using the R programming language, with
513 visualization facilitated by the gplots package. Visualization of peaks across the full length of LINE1
514 was achieved through the UCSC Genome Browser.74.
515
516 **Supplemental Information**
517 Supplemental Tables 2
518 Supplemental Figures 1-5
519
520 **Acknowledgements**
521 This work was supported by the DBT/Wellcome Trust India Alliance fellowship (IA/I/22/2/506501) to
522 Bhavana Tiwari. Pratyashaa Paul was supported by IISER Berhampur, (A.K) CSIR-JRF, (A.K.D)
523 UGC-JRF. The authors would also like to acknowledge the assistance of ILS Bhubaneswar confocal
524 imaging facility and the imaging facility UTSW, Dallas, Texas for microscopy. We acknowledge Prof.

525 John Abrams at the Department of Cell Biology, University of Texas Southwestern Medical Center,
526 Texas for generously providing chemicals, reagents, including wt and p53 ko cells, as well as plasmid
527 resources utilized in this study. We thank Dr. Amanda Jones and Prof. John Abrams of UTSW, Texas
528 for valuable suggestions. Illustration work for graphical abstract was created with BioRender.com.
529 We thank IISER Berhampur for the support.
530

531 **Contributions**

532 BT conceived the studies. PP, AK, AKD, AP, GP, FP and BT performed experiments and analysed
533 data. SK processed the microscopy data and assisted in the illustration of the graphical abstract. BT
534 designed the study, analysed data, and both BT and PP wrote the manuscript.
535

536 **Declaration of interests**

537 The authors declare no competing interests.
538

539 **Figure legends**
540

541 **Figure 1. Elevation of L1 encoded intermediate components in p53$^{-/-}$ cells:**
542 **(**A-B) qRT-PCR analyses was performed using the primers that detects consensus sequences of
543 5'UTR, L1ORF1 and L1ORF2 transcripts in wt and p53$^{-/-}$ of (A) A375 and (B) U2OS cells. The
544 transcript levels were normalized using ß-actin and relative fold change was calculated with respect
545 to the parental wild type. The data shown are the averages of three biological replicates. *$p<0.05$,
546 **$p<0.01$, (Mann-Whitney U test).

547 (C-D) Representative confocal images display immunofluorescence staining for L1-ORF1p (Alexa
548 Fluor 568, red) and DAPI (blue) in wt and p53$^{-/-}$ cells of (C) A375 and (D) U2OS. Scale bars, 100
549 µm and 30 µm respectively.

550 (E) Immunofluorescence images s9.6 stained (Alexa Fluor, 488) and DAPI (blue) A375 wt and p53^{-}
551 $^{/-}$ cells. Scale bar,100 µm. Shown images are representative of three biological replicates.

552 (E') Quantification of s9.6 intensities of whole cell from A375 p53 wt and p53$^{-/-}$ using fiji. Minimum 60
553 cells were analysed for RNA-DNA hybrid quantification from three biological replicates. *$p<0.05$,
554 ns=non-significant (Mann-Whitney U test).

555 (F) DRIP-qPCR was performed to measure R-loops in A375 p53 wt and p53$^{-/-}$ cells.
556 Immunoprecipitation carried out using the s9.6 antibody. Arrows at the schematic indicate to primers
557 amplifying different regions of L1 sequence at 5'-UTR, ORF1 and ORF2). RPL13A was used a
558 positive control for quantification of the R-loop locus and ZNF544 as negative locus. Enrichment of
559 RNA-DNA hybrids in each region, normalized to input values. Data represent mean± S.D. from three
560 biological experiments. *p<0.05, ns=non-significant (Mann-Whitney U test).

561 (G) The representative fluorescent images show A375 wt and p53$^{-/-}$ cells transfected with RNaseH1
562 D210N-GFP (RNH-GFP) construct. The nuclear foci indicate the expression of RNaseH1 D210N-
563 GFP (RNH-GFP, green), nucleus (Blue).

564 (H) DRIP-qPCR on RNaseH D210N-GFP stably transfected cells of A375 wt and p53$^{-/-}$ cells using
565 the primers detecting L1-5'UTR, ORF1 and ORF2 loci. RPL13A used as a positive control for the R-
566 loop enrichment and ZNF544 as negative locus. Signal values of RNA-DNA hybrids
567 immunoprecipitated in each region, normalized to input values. Data represent mean±S.D. from the
568 three independent experiments. *p<0.05, ns=non-significant (Mann-Whitney U test).

569 (I) This figure illustrates the comparison of DRIP-seq signals in the input control and
570 immunoprecipitated sample, as well as the GRO-seq signal from the same cell line. The analyses
571 from the dataset (PMID 26579211) focuses on a specific L1Hs genomic region. The green peak
572 corresponds to the input of DRIP-seq data, whereas the blue peaks reflects the DRIP-sequenced
573 data obtained from s9.6 immunoprecipitated HEK293T cells. The orange curve indicates Gro-seq
574 data from HEK293T cells to quantify nascent RNAs at L1. The depicted schematic shows the L1
575 regions: 5'UTR, ORF1, and ORF2 (represented by black bars). The data also provides insights on
576 the genomic locations of L1 in chromosome 7 of the hg38 assembly.

577

578 **Figure 2. Increased accumulation of L1 trans R-loops derived RNA-DNA hybrids in p53$^{-/-}$**
579 (A) Heat map shows R-loops enrichment in human TE families obtained from the DRIP-seq data
580 analysis. Each row represents a TE family grouped according to their repBase classification. The L1
581 has been classified as per their age, e.g. L1-young are full length sequences and are capable of
582 retrotransposition including the loci from L1Hs family. Rows are clustered using the K-means
583 algorithm and columns represent the sample types (with p53 status of the cells). The legend
584 represents the differential presence of various TE families in the sample. Adjusted p-value of the

585 Table is 0.05. Sample 1 (SRR2028291), 2 (SRR2028292), 3 (SRR5137197), 4 (SRR5137200), 5
586 (SRR2028293), 6 (SRR2028294), 7 (SRR9937575), 8 (SRR9937576).
587
588 (B) Full-length L1 transcript analyses were performed in SW480 cell line (green) treated with NaB
589 and from human pancreatic islets (HPI, yellow) treated with TSA (PMID: 38410440, 38410440).
590 (Mann-Whitney U Test, *p<0.05). These cell lines are reported to harbour p53 mutation.
591
592 (C) qRT-PCR analysis of L1 ORF1 expression of A375 wt and $p53^{-/-}$ upon NaB treatment. The data
593 shown are the averages of three biological replicates (Mann-Whitney U Test, *p<0.05, **p<0.01).
594
595 (D) Illustration of strategies involving DMSO or NaB drug (25 µm) treatment on A375 wt and $p53^{-/-}$,
596 as indicated for 24 hours, followed by drug withdrawal for 4 and 7 days. Cell viability was assessed
597 through cell glow titre experiments at (1 day, 3 days and 7 of drug treatment) (**Supplemental Figure**
598 **S3A**) to measure HDACi drug toxicity.
599
600 (E) Representative immunofluorescence microscopy images of three biological replicates showing
601 RNA-DNA hybrid accumulation in wt and $p53^{-/-}$ A375 cells after treatment with either DMSO or NaB
602 for 24 hours, followed by 3TC treatment for 72 hours. Scale bar indicates 50 um.
603
604 (E') Quantification of s9.6 intensities from the whole cells was done using Fiji software [62]. Violin plots
605 exhibit combined data from three biological replicates with p values determined by Mann–Whitney
606 test. p<0.05,*p<0.01. A minimum of 50 cells were measured in each sample of the three biological
607 replicates.
608
609 (F) DRIP-qPCR was performed to measure R-loops in A375 p53 wt and $p53^{-/-}$ cells upon 3TC
610 treatment. Immunoprecipitation carried out using the s9.6 antibody. Enrichment of RNA-DNA hybrids
611 in each region, normalized to input values. Data represent mean±S.D. from three independent
612 experiments. *p<0.05, ns=non-significant (Mann-Whitney U test).
613
614 (G) DRIP-qPCR on RNaseH D210N-GFP stably transfected cells of A375 p53 wt and $p53^{-/-}$ cells
615 upon 3TC treatment. Immunoprecipitation carried out using the GFP antibody. Enrichment of RNA-
616 DNA hybrids in each region, normalized to input values. Data represent mean±S.D. from three
617 independent experiments. *p<0.05, ns = non-significant (Mann-Whitney U test).
618 **Figure 3. Effect of reverse transcriptase inhibitor on RT domain overexpressing $p53^{-/-}$ cells**

619 (A) Representative fluorescence images depict the transient overexpression of A375 p53$^{-/-}$ cells with
620 pEGFP-N1 (EV), L1-ORF1p, Endonuclease (EN), Reverse Transcriptase (RT) domains of L1-
621 ORF2p followed by 3TC treatment for 3 days post transfection of 24 h. The overexpressed proteins
622 are c-terminally GFP tagged (green) and s9.6 (red) that visualize RNA-DNA hybrids are mostly
623 localised at the cytoplasm, nucleus is stained with DAPI (blue). Scale bar represents 50um.
624
625 (B) The heatmap shows a consolidated qRT-PCR of DNA repair genes (RAD50, BRCA1, Rb) and
626 inflammatory markers (STING, IRF7, MCP, CXCL10, IFNβ, ISG15) from the exogenously expressed
627 ORF1p, EN domain, RT domain in A375 p53$^{-/-}$ cells followed by 3TC treatment for 3 days. The
628 subsequent legend shows the level of expression following overexpression. The samples were
629 harvested after 3TC treatment for 3 days on 24 h transfected cells. The data from three biological
630 replicates were included for heatmap generation. The normalised p-value of the data is less than
631 0.05.
632
633 (C) Sequential DRIP-qPCR was performed on RT-GFP exogenously overexpressing A375 p53$^{-/-}$
634 followed by DMSO or 3TC treatment for 3 days. The first round of immunoprecipitation was
635 performed using GFP antibody followed by another round of immunoprecipitation by s9.6 on the
636 GFP immunoprecipitated samples. Enrichment of RNA-DNA hybrids in each sample, normalized to
637 the respective input values. Data represent mean±S.D. from the three independent experiments.
638
639 (D) Representative confocal images of EV, EN, RT (all GFP tagged) transiently overexpressing p53^{-}
640 $^{/-}$ cells (green) and yH2AX foci (red) localised at the nucleus (DAPI, blue). The merged images show
641 overlap of yH2AX , DAPI , GFP. Scale bar represents 50um.
642
643 (D') Violin plots represent the y2AX (red) foci quantification. yH2AX foci were quantified via Fiji
644 software. The mean (black line) represent the average foci from 50 nuclei. The data was quantified
645 using fiji between three biological replicates. *p<0.05 (Mann-Whitney U test).
646
647 **Figure 4. The dynamics of the L1-5'UTR-eGFP reporter upon exposure to HDAC inhibitors**
648 **and subsequent drug withdrawal.**
649 (A) Illustrates the schematic of TSA drug treatment and withdrawal in U2OS wt and p53$^{-/-}$ cells. The samples
650 were collected for qRT-PCR, western blotting, and microscopy at 24 hours post-drug (HDACi) treatment, as
651 well as at 4 and 7 days. TSA and NaB denote drug treatment for 24 hours, TSA-4D and NaB-4D indicate

652 drug withdrawal of 3 days, and TSA-7D and NaB-7D signify withdrawal after 6 days post 24-hour treatment
653 (L1-ORF1; 568, GFP; 488, and DAPI channels).
654
655 (B) Confocal imaging of GFP and RNA *in situ* hybridization of L1-ORF1 using Stellaris probes (from
656 LGC Biosearch Technologies) was performed in wt and p53$^{-/-}$ U2OS cells harbouring L1-5'UTR-
657 eGFP construct. The reporter cells were treated with either DMSO or TSA for 24 hours, followed by
658 withdrawal for 3 and 6 days. Samples were collected at 1 day, 4 days, and 7 days for confocal
659 imaging post HDACi treatment for GFP activation and silencing. Presented here are representative
660 confocal images from three independent immunofluorescence experiments. Activation of L1-ORF1
661 transcripts was visualised using Qusar 570 Stellaris probes sequences (**Supplementary Table 2**).
662 Scale bar indicates 20 um.
663
664 (C-D) RT-qPCR analysis was performed to quantify L1-ORF1 and gfp transcripts in wt and p53$^{-/-}$ L1-
665 5'UTR cells treated with DMSO or TSA/NaB at 1, 4 and 7 days. The data represent the mean ±
666 standard deviation (S.D.) from three independent biological replicates (n=3). *$p<0.05$, **$p<0.01$,
667 ns=non-significant. (Mann-Whitney U test). The primers used for qPCR analysis of ORF1 and egfp
668 transcripts are provided in **Supplemental Table 1.**
669
670 (E-F) Western blotting of H3Ac and total H3 levels (E) and H4Ac and H4 total levels (F) in U2OS wt
671 and p53$^{-/-}$ cells upon either DMSO or TSA 24 h treatment.
672
673 **Figure 5. p53 facilitates the rapid re-establishment of LRE3 silencing, a retrotransposition**
674 **indicator, following withdrawal of HDACi drugs.**
675 (A) Illustrates the schematic representation of DMSO, TSA/NaB drug treatment and subsequent
676 withdrawal in U2OS wt and p53$^{-/-}$ cells.
677
678 (B) Illustrations indicates the nature of LRE3 plasmid which is a surrogate marker of
679 retrotransposition. Cells that undergo retrotransposition are GFP positive (green).
680
681 (C-D) The representative confocal images demonstrate the expression of GFP (green) in U2OS wt
682 and p53$^{-/-}$ cells following exposure to TSA (C) and NaB (D) drugs for 24 hours, followed by drug
683 withdrawal of 3 or 6 days. Scale bar indicates 20um and the experiments were conducted with 3
684 biological replicates.

685 (C'-D') Percentage of GFP positive cells in U2OS wt and p53$^{-/-}$ at 24 hrs of TSA (C) and NaB (D)
686 treatment followed by drug withdrawal at 3 and 6 days. GFP positive cells were counted from
687 minimum 10 fields from the 3 independent experiments. The error bar represents mean of 3
688 biological replicates. *p<0.05, **p<0.01, ns=non-significant (Mann-Whitney U test).
689
690 **Figures 6. Histone modification dynamics in L1-5'UTR-eGFP reporter cells upon HDACi**
691 **exposure and withdrawal**
692 (A-C) Chromatin immunoprecipitation followed by qPCR analyses was conducted on the 5'UTR
693 region of A375 wt and p53$^{-/-}$ L1-5'UTR-eGFP stable cells. Primers targeting the p53 binding region
694 were utilized, with immunoprecipitation carried out using antibodies against histone modifications
695 H3K9me3, H3K27me3, H3K9Ac, and H3K4me3. The results illustrate normalized levels of H3K9me3
696 and H3K27me3, representative of repressive histone marks (A and B), normalized to input values,
697 as well as levels of activation marks H3K9Ac (C) and H3K4me3 (D). Reporter cells were treated with
698 HDACi for 24 h followed by withdrawal for 3 and 6 days. Samples for analyses were collected at 1
699 day, 4 and 7 days (for drug withdrawal), as depicted (refer to **Figures** 4 and 5). It is noteworthy that
700 alterations in H3K9me3, H3K27me3, H3K9Ac, and H3K4me3 enrichment are specific to the p53
701 status. Error bars represent the standard error of the mean from three biological replicates. *p<0.05,
702 **p<0.01, ns=non-significant (Mann-Whitney U test).
703
704 **Figure 7. Effect of 3TC on L1-ORF1p expression and 53BP-1 foci**
705 (A) Confocal imaging of L1-ORF1p (green), 53BP-1 (magenta, foci indicated in white) and nucleus
706 (blue) in U2OS wt and lacking p53 were treated with either DMSO or TSA for 24 hours, followed by
707 3TC treatment for 3 and 6 days. Imaging of cells performed at 1 day after TSA exposure, and at 3
708 and 6 days after 3TC treatment. Presented here are representative confocal images from three
709 independent immunofluorescence imaging experiments. Upon 24-hour exposure to TSA, activation
710 of L1-ORF1p and accumulation of 53BP-1 foci (indicated by white arrows) were observed.
711 Conversely, suppression of L1-ORF1p and reduction of 53BP-1 foci were more evident in wt than
712 p53$^{-/-}$ cells after 3 and 6 days of 3TC treatment. Scale bar denotes 20um.
713
714 (A') The Violin plot shows the quantified 53BP1 foci from microscopy images. The bold dotted line
715 represent the mean foci from 50 different nuclei. The quantification has been done from 3 different
716 biological replicates. *p<0.05, ns=non-significant (Mann-Whitney U test).
717
718

References

1. Soussi, T., and Wiman, K.G. (2015). TP53: an oncogene in disguise. Cell death and differentiation *22*, 1239-1249. 10.1038/cdd.2015.53.
2. Vousden, K.H., and Lane, D.P. (2007). p53 in health and disease. Nat Rev Mol Cell Biol *8*, 275-283. 10.1038/nrm2147.
3. McKerrow, W., Wang, X., Mendez-Dorantes, C., Mita, P., Cao, S., Grivainis, M., Ding, L., LaCava, J., Burns, K.H., Boeke, J.D., and Fenyo, D. (2022). LINE-1 expression in cancer correlates with p53 mutation, copy number alteration, and S phase checkpoint. Proc Natl Acad Sci U S A *119*. 10.1073/pnas.2115999119.
4. Tiwari, B., Jones, A.E., Caillet, C.J., Das, S., Royer, S.K., and Abrams, J.M. (2020). p53 directly represses human LINE1 transposons. Genes Dev. 10.1101/gad.343186.120.
5. Rodriguez-Martin, B., Alvarez, E.G., Baez-Ortega, A., Zamora, J., Supek, F., Demeulemeester, J., Santamarina, M., Ju, Y.S., Temes, J., Garcia-Souto, D., et al. (2020). Pan-cancer analysis of whole genomes identifies driver rearrangements promoted by LINE-1 retrotransposition. Nat Genet *52*, 306-319. 10.1038/s41588-019-0562-0.
6. Shin, Y.J., Kim, Y., Wen, X., Cho, N.Y., Lee, S., Kim, W.H., and Kang, G.H. (2019). Prognostic implications and interaction of L1 methylation and p53 expression statuses in advanced gastric cancer. Clin Epigenetics *11*, 77. 10.1186/s13148-019-0661-x.
7. Wylie, A., Jones, A.E., D'Brot, A., Lu, W.J., Kurtz, P., Moran, J.V., Rakheja, D., Chen, K.S., Hammer, R.E., Comerford, S.A., et al. (2016). p53 genes function to restrain mobile elements. Genes Dev *30*, 64-77. 10.1101/gad.266098.115.
8. Tiwari, B., Kurtz, P., Jones, A.E., Wylie, A., Amatruda, J.F., Boggupalli, D.P., Gonsalvez, G.B., and Abrams, J.M. (2017). Retrotransposons Mimic Germ Plasm Determinants to Promote Transgenerational Inheritance. Curr Biol *27*, 3010-3016 e3013. 10.1016/j.cub.2017.08.036.
9. Tiwari, B., Jones, A.E., Caillet, C.J., Das, S., Royer, S.K., and Abrams, J.M. (2020). p53 directly represses human LINE1 transposons. Genes Dev *34*, 1439-1451. 10.1101/gad.343186.120.
10. Tiwari, B., Jones, A.E., and Abrams, J.M. (2018). Transposons, p53 and Genome Security. Trends Genet *34*, 846-855. 10.1016/j.tig.2018.08.003.
11. Harris, C.R., Dewan, A., Zupnick, A., Normart, R., Gabriel, A., Prives, C., Levine, A.J., and Hoh, J. (2009). p53 responsive elements in human retrotransposons. Oncogene *28*, 3857-3865. 10.1038/onc.2009.246.

752 12. Zemojtel, T., Kielbasa, S.M., Arndt, P.F., Chung, H.R., and Vingron, M. (2009). Methylation
753 and deamination of CpGs generate p53-binding sites on a genomic scale. Trends Genet *25*,
754 63-66. 10.1016/j.tig.2008.11.005.
755 13. Cui, F., Sirotin, M.V., and Zhurkin, V.B. (2011). Impact of Alu repeats on the evolution of
756 human p53 binding sites. Biol Direct *6*, 2. 10.1186/1745-6150-6-2.
757 14. Ardeljan, D., Taylor, M.S., Ting, D.T., and Burns, K.H. (2017). The Human Long Interspersed
758 Element-1 Retrotransposon: An Emerging Biomarker of Neoplasia. Clin Chem *63*, 816-822.
759 10.1373/clinchem.2016.257444.
760 15. Burns, K.H. (2017). Transposable elements in cancer. Nat Rev Cancer *17*, 415-424.
761 10.1038/nrc.2017.35.
762 16. Brunmeir, R., Lagger, S., Simboeck, E., Sawicka, A., Egger, G., Hagelkruys, A., Zhang, Y.,
763 Matthias, P., Miller, W.J., and Seiser, C. (2010). Epigenetic regulation of a murine
764 retrotransposon by a dual histone modification mark. PLoS Genet *6*, e1000927.
765 10.1371/journal.pgen.1000927.
766 17. Garcia-Perez, J.L., Morell, M., Scheys, J.O., Kulpa, D.A., Morell, S., Carter, C.C., Hammer,
767 G.D., Collins, K.L., O'Shea, K.S., Menendez, P., and Moran, J.V. (2010). Epigenetic silencing
768 of engineered L1 retrotransposition events in human embryonic carcinoma cells. Nature *466*,
769 769-773. 10.1038/nature09209.
770 18. Gaillard, S.L., Zahurak, M., Sharma, A., Durham, J.N., Reiss, K.A., Sartorius-Mergenthaler,
771 S., Downs, M., Anders, N.M., Ahuja, N., Rudek, M.A., and Azad, N. (2019). A phase 1 trial of
772 the oral DNA methyltransferase inhibitor CC-486 and the histone deacetylase inhibitor
773 romidepsin in advanced solid tumors. Cancer *125*, 2837-2845. 10.1002/cncr.32138.
774 19. Rodriguez-Martin, B., Alvarez, E.G., Baez-Ortega, A., Zamora, J., Supek, F.,
775 Demeulemeester, J., Santamarina, M., Ju, Y.S., Temes, J., Garcia-Souto, D., et al. (2020).
776 Pan-cancer analysis of whole genomes identifies driver rearrangements promoted by LINE-
777 1 retrotransposition. Nat Genet *52*, 306-319. 10.1038/s41588-019-0562-0.
778 20. Goodier, J.L. (2016). Restricting retrotransposons: a review. Mob DNA *7*, 16.
779 10.1186/s13100-016-0070-z.
780 21. Rodic, N., Sharma, R., Sharma, R., Zampella, J., Dai, L., Taylor, M.S., Hruban, R.H.,
781 Iacobuzio-Donahue, C.A., Maitra, A., Torbenson, M.S., et al. (2014). Long interspersed
782 element-1 protein expression is a hallmark of many human cancers. Am J Pathol *184*, 1280-
783 1286. 10.1016/j.ajpath.2014.01.007.
784 22. Crow, M.K. (2010). Long interspersed nuclear elements (LINE-1): potential triggers of
785 systemic autoimmune disease. Autoimmunity *43*, 7-16. 10.3109/08916930903374865.

786 23. Subbalekha, K., Pimkhaokham, A., Pavasant, P., Chindavijak, S., Phokaew, C.,
787 Shuangshoti, S., Matangkasombut, O., and Mutirangura, A. (2009). Detection of LINE-1s
788 hypomethylation in oral rinses of oral squamous cell carcinoma patients. Oral Oncol *45*, 184-
789 191. 10.1016/j.oraloncology.2008.05.002.
790 24. Baldwin, E.T., van Eeuwen, T., Hoyos, D., Zalevsky, A., Tchesnokov, E.P., Sanchez, R.,
791 Miller, B.D., Di Stefano, L.H., Ruiz, F.X., Hancock, M., et al. (2024). Structures, functions and
792 adaptations of the human LINE-1 ORF2 protein. Nature *626*, 194-206. 10.1038/s41586-023-
793 06947-z.
794 25. De Cecco, M., Ito, T., Petrashen, A.P., Elias, A.E., Skvir, N.J., Criscione, S.W., Caligiana, A.,
795 Brocculi, G., Adney, E.M., Boeke, J.D., et al. (2019). L1 drives IFN in senescent cells and
796 promotes age-associated inflammation. Nature *566*, 73-78. 10.1038/s41586-018-0784-9.
797 26. Gan, W., Guan, Z., Liu, J., Gui, T., Shen, K., Manley, J.L., and Li, X. (2011). R-loop-mediated
798 genomic instability is caused by impairment of replication fork progression. Genes Dev *25*,
799 2041-2056. 10.1101/gad.17010011.
800 27. Crossley, M.P., Bocek, M., and Cimprich, K.A. (2019). R-Loops as Cellular Regulators and
801 Genomic Threats. Molecular cell *73*, 398-411. 10.1016/j.molcel.2019.01.024.
802 28. Wells, J.P., White, J., and Stirling, P.C. (2019). R Loops and Their Composite Cancer
803 Connections. Trends Cancer *5*, 619-631. 10.1016/j.trecan.2019.08.006.
804 29. Stirling, P.C., Chan, Y.A., Minaker, S.W., Aristizabal, M.J., Barrett, I., Sipahimalani, P., Kobor,
805 M.S., and Hieter, P. (2012). R-loop-mediated genome instability in mRNA cleavage and
806 polyadenylation mutants. Genes Dev *26*, 163-175. 10.1101/gad.179721.111.
807 30. Wood, M., Quinet, A., Lin, Y.L., Davis, A.A., Pasero, P., Ayala, Y.M., and Vindigni, A. (2020).
808 TDP-43 dysfunction results in R-loop accumulation and DNA replication defects. J Cell Sci
809 *133*. 10.1242/jcs.244129.
810 31. Crossley, M.P., Song, C., Bocek, M.J., Choi, J.H., Kousouros, J.N., Sathirachinda, A., Lin,
811 C., Brickner, J.R., Bai, G., Lans, H., et al. (2023). R-loop-derived cytoplasmic RNA-DNA
812 hybrids activate an immune response. Nature *613*, 187-194. 10.1038/s41586-022-05545-9.
813 32. Dewannieux, M., Esnault, C., and Heidmann, T. (2003). LINE-mediated retrotransposition of
814 marked Alu sequences. Nat Genet *35*, 41-48. 10.1038/ng1223.
815 33. Kajikawa, M., and Okada, N. (2002). LINEs mobilize SINEs in the eel through a shared 3'
816 sequence. Cell *111*, 433-444. 10.1016/s0092-8674(02)01041-3.
817 34. Hancks, D.C., Goodier, J.L., Mandal, P.K., Cheung, L.E., and Kazazian, H.H., Jr. (2011).
818 Retrotransposition of marked SVA elements by human L1s in cultured cells. Hum Mol Genet
819 *20*, 3386-3400. 10.1093/hmg/ddr245.

820 35. Ostertag, E.M., Goodier, J.L., Zhang, Y., and Kazazian, H.H., Jr. (2003). SVA elements are
821 nonautonomous retrotransposons that cause disease in humans. Am J Hum Genet *73*, 1444-
822 1451. 10.1086/380207.
823 36. Anwar, S.L., Wulaningsih, W., and Lehmann, U. (2017). Transposable Elements in Human
824 Cancer: Causes and Consequences of Deregulation. Int J Mol Sci *18*.
825 10.3390/ijms18050974.
826 37. Imperatori, A., Sahnane, N., Rotolo, N., Franzi, F., Nardecchia, E., Libera, L., Romualdi, C.,
827 Cattoni, M., Sessa, F., Dominioni, L., and Furlan, D. (2017). LINE-1 hypomethylation is
828 associated to specific clinico-pathological features in Stage I non-small cell lung cancer. Lung
829 Cancer *108*, 83-89. 10.1016/j.lungcan.2017.03.003.
830 38. Briggs, E.M., Ha, S., Mita, P., Brittingham, G., Sciamanna, I., Spadafora, C., and Logan, S.K.
831 (2018). Long interspersed nuclear element-1 expression and retrotransposition in prostate
832 cancer cells. Mob DNA *9*, 1. 10.1186/s13100-017-0106-z.
833 39. Skourti-Stathaki, K. (2022). Detection of R-Loop Structures by Immunofluorescence Using
834 the S9.6 Monoclonal Antibody. Methods Mol Biol *2528*, 21-29. 10.1007/978-1-0716-2477-
835 7_2.
836 40. Sanz, L.A., and Chedin, F. (2019). High-resolution, strand-specific R-loop mapping via S9.6-
837 based DNA-RNA immunoprecipitation and high-throughput sequencing. Nat Protoc *14*,
838 1734-1755. 10.1038/s41596-019-0159-1.
839 41. Ginno, P.A., Lott, P.L., Christensen, H.C., Korf, I., and Chedin, F. (2012). R-loop formation is
840 a distinctive characteristic of unmethylated human CpG island promoters. Molecular cell *45*,
841 814-825. 10.1016/j.molcel.2012.01.017.
842 42. Lin, R., Zhong, X., Zhou, Y., Geng, H., Hu, Q., Huang, Z., Hu, J., Fu, X.D., Chen, L., and
843 Chen, J.Y. (2022). R-loopBase: a knowledgebase for genome-wide R-loop formation and
844 regulation. Nucleic Acids Res *50*, D303-D315. 10.1093/nar/gkab1103.
845 43. Yan, Q., Shields, E.J., Bonasio, R., and Sarma, K. (2019). Mapping Native R-Loops Genome-
846 wide Using a Targeted Nuclease Approach. Cell reports *29*, 1369-1380 e1365.
847 10.1016/j.celrep.2019.09.052.
848 44. Templeton, C.W., and Laimins, L.A. (2023). p53-dependent R-loop formation and HPV
849 pathogenesis. Proc Natl Acad Sci U S A *120*, e2305907120. 10.1073/pnas.2305907120.
850 45. Panatta, E., Butera, A., Mammarella, E., Pitolli, C., Mauriello, A., Leist, M., Knight, R.A.,
851 Melino, G., and Amelio, I. (2022). Metabolic regulation by p53 prevents R-loop-associated
852 genomic instability. Cell reports *41*, 111568. 10.1016/j.celrep.2022.111568.

853 46. Kopera, H.C., Larson, P.A., Moldovan, J.B., Richardson, S.R., Liu, Y., and Moran, J.V.
854 (2016). LINE-1 Cultured Cell Retrotransposition Assay. Methods Mol Biol *1400*, 139-156.
855 10.1007/978-1-4939-3372-3_10.
856 47. Ostertag, E.M., Prak, E.T., DeBerardinis, R.J., Moran, J.V., and Kazazian, H.H., Jr. (2000).
857 Determination of L1 retrotransposition kinetics in cultured cells. Nucleic Acids Res *28*, 1418-
858 1423. 10.1093/nar/28.6.1418.
859 48. Lee, J.H., Choy, M.L., Ngo, L., Foster, S.S., and Marks, P.A. (2010). Histone deacetylase
860 inhibitor induces DNA damage, which normal but not transformed cells can repair. Proc Natl
861 Acad Sci U S A *107*, 14639-14644. 10.1073/pnas.1008522107.
862 49. Rodriguez-Martin, B., Alvarez, E.G., Baez-Ortega, A., Zamora, J., Supek, F.,
863 Demeulemeester, J., Santamarina, M., Ju, Y.S., Temes, J., Garcia-Souto, D., et al. (2020).
864 Pan-cancer analysis of whole genomes identifies driver rearrangements promoted by LINE-
865 1 retrotransposition. Nat Genet. 10.1038/s41588-019-0562-0.
866 50. Simon, M., Van Meter, M., Ablaeva, J., Ke, Z., Gonzalez, R.S., Taguchi, T., De Cecco, M.,
867 Leonova, K.I., Kogan, V., Helfand, S.L., et al. (2019). LINE1 Derepression in Aged Wild-Type
868 and SIRT6-Deficient Mice Drives Inflammation. Cell Metab *29*, 871-885 e875.
869 10.1016/j.cmet.2019.02.014.
870 51. Hegazy, Y.A., Fernando, C.M., and Tran, E.J. (2020). The balancing act of R-loop biology:
871 The good, the bad, and the ugly. J Biol Chem *295*, 905-913. 10.1074/jbc.REV119.011353.
872 52. Hontecillas-Prieto, L., Flores-Campos, R., Silver, A., de Alava, E., Hajji, N., and Garcia-
873 Dominguez, D.J. (2020). Synergistic Enhancement of Cancer Therapy Using HDAC
874 Inhibitors: Opportunity for Clinical Trials. Front Genet *11*, 578011.
875 10.3389/fgene.2020.578011.
876 53. Bregnard, C., Guerra, J., Dejardin, S., Passalacqua, F., Benkirane, M., and Laguette, N.
877 (2016). Upregulated LINE-1 Activity in the Fanconi Anemia Cancer Susceptibility Syndrome
878 Leads to Spontaneous Pro-inflammatory Cytokine Production. EBioMedicine *8*, 184-194.
879 10.1016/j.ebiom.2016.05.005.
880 54. Saleh, A., Macia, A., and Muotri, A.R. (2019). Transposable Elements, Inflammation, and
881 Neurological Disease. Front Neurol *10*, 894. 10.3389/fneur.2019.00894.
882 55. Leonova, K.I., Brodsky, L., Lipchick, B., Pal, M., Novototskaya, L., Chenchik, A.A., Sen, G.C.,
883 Komarova, E.A., and Gudkov, A.V. (2013). p53 cooperates with DNA methylation and a
884 suicidal interferon response to maintain epigenetic silencing of repeats and noncoding RNAs.
885 Proc Natl Acad Sci U S A *110*, E89-98. 10.1073/pnas.1216922110.

886 56. Jones, R.B., Garrison, K.E., Wong, J.C., Duan, E.H., Nixon, D.F., and Ostrowski, M.A.
887 (2008). Nucleoside analogue reverse transcriptase inhibitors differentially inhibit human
888 LINE-1 retrotransposition. PLoS One *3*, e1547. 10.1371/journal.pone.0001547.
889 57. Dai, L., Huang, Q., and Boeke, J.D. (2011). Effect of reverse transcriptase inhibitors on LINE-
890 1 and Ty1 reverse transcriptase activities and on LINE-1 retrotransposition. BMC Biochem
891 *12*, 18. 10.1186/1471-2091-12-18.
892 58. Banuelos-Sanchez, G., Sanchez, L., Benitez-Guijarro, M., Sanchez-Carnerero, V., Salvador-
893 Palomeque, C., Tristan-Ramos, P., Benkaddour-Boumzaouad, M., Morell, S., Garcia-Puche,
894 J.L., Heras, S.R., et al. (2019). Synthesis and Characterization of Specific Reverse
895 Transcriptase Inhibitors for Mammalian LINE-1 Retrotransposons. Cell Chem Biol *26*, 1095-
896 1109 e1014. 10.1016/j.chembiol.2019.04.010.
897 59. Nishikawa, S., and Iwakuma, T. (2023). Drugs Targeting p53 Mutations with FDA Approval
898 and in Clinical Trials. Cancers (Basel) *15*. 10.3390/cancers15020429.
899 60. Crossley, M.P., Brickner, J.R., Song, C., Zar, S.M.T., Maw, S.S., Chedin, F., Tsai, M.S., and
900 Cimprich, K.A. (2021). Catalytically inactive, purified RNase H1: A specific and sensitive
901 probe for RNA-DNA hybrid imaging. J Cell Biol *220*. 10.1083/jcb.202101092.
902 61. Bao, W., Kojima, K.K., and Kohany, O. (2015). Repbase Update, a database of repetitive
903 elements in eukaryotic genomes. Mob DNA *6*, 11. 10.1186/s13100-015-0041-9.
904 62. Schindelin, J., Arganda-Carreras, I., Frise, E., Kaynig, V., Longair, M., Pietzsch, T., Preibisch,
905 S., Rueden, C., Saalfeld, S., Schmid, B., et al. (2012). Fiji: an open-source platform for
906 biological-image analysis. Nat Methods *9*, 676-682. 10.1038/nmeth.2019.
907

Graphical

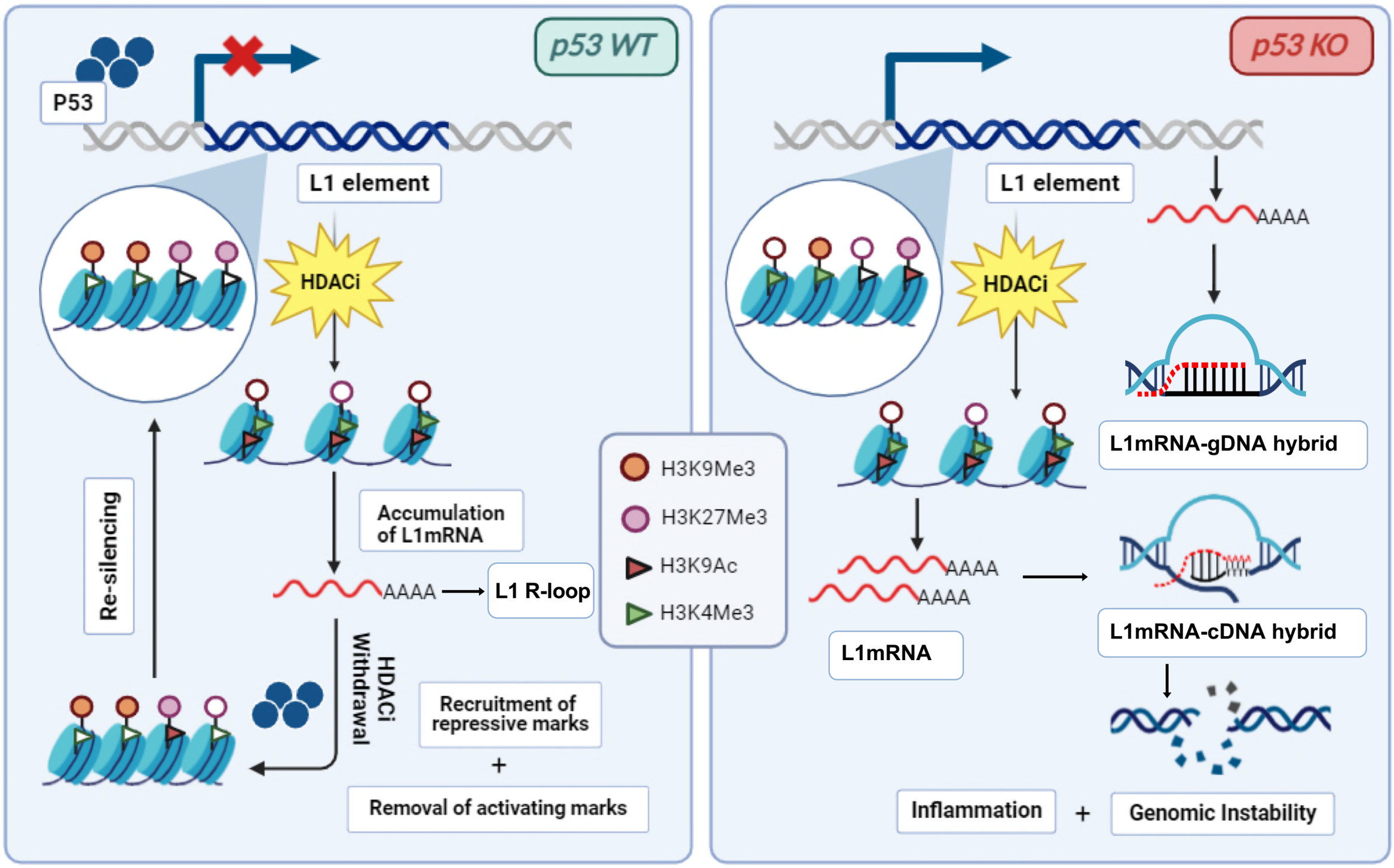
p53 WT
P53
L1 element
HDACi
Accumulation of L1mRNA
AAAA
L1 R-loop
Re-silencing
HDACi Withdrawal
Recruitment of repressive marks
+
Removal of activating marks
H3K9Me3
H3K27Me3
H3K9Ac
H3K4Me3
p53 KO
L1 element
AAAA
HDACi
L1mRNA-gDNA hybrid
AAAA
AAAA
L1mRNA
L1mRNA-cDNA hybrid
Inflammation
+
Genomic Instability

Figure 1

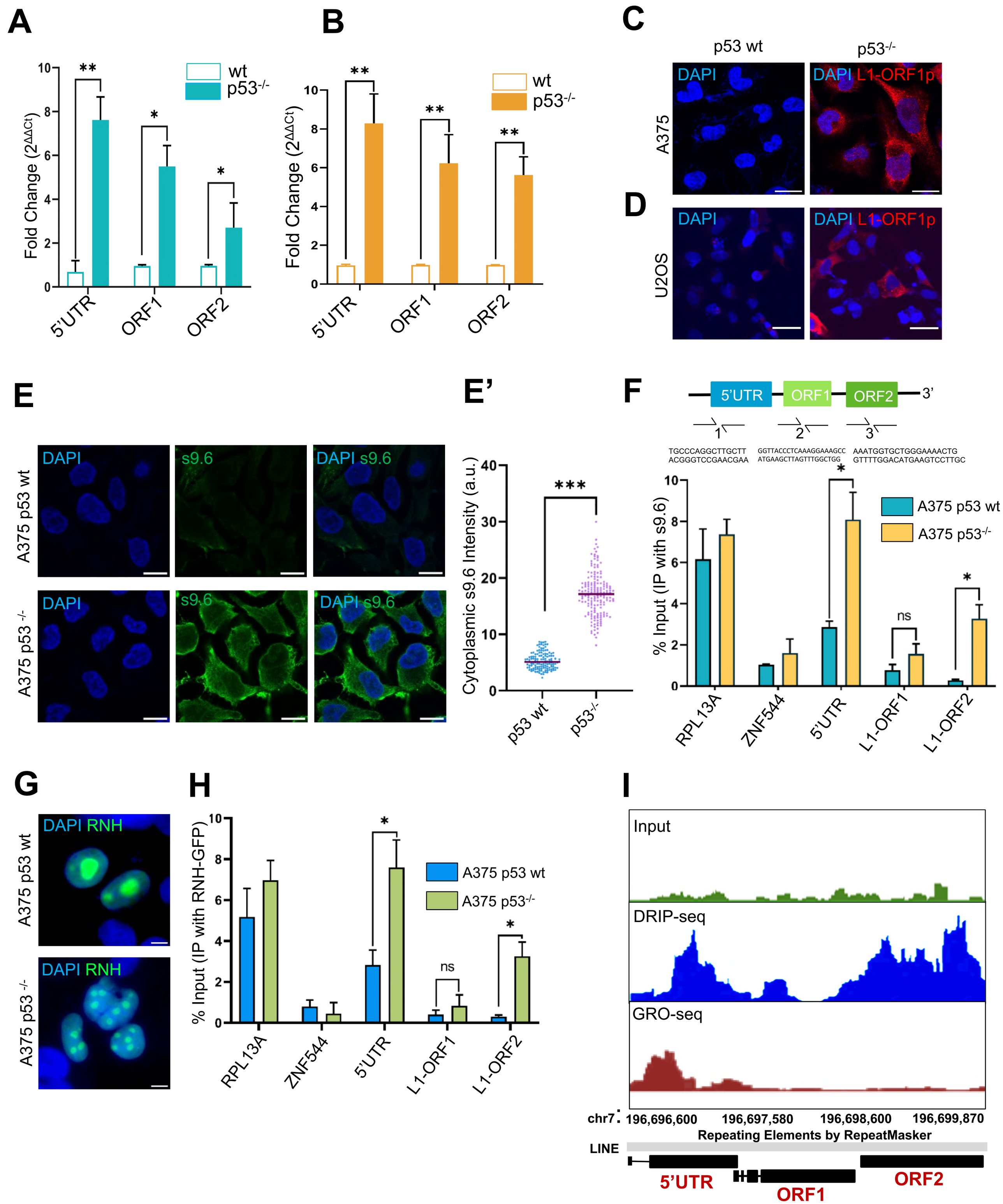
A
B
C
D
E
E'
F
G
H
I
wt
p53-/-
Fold Change (2ΔΔCt)
5'UTR
ORF1
ORF2
p53 wt
p53-/-
DAPI
L1-ORF1p
A375
U2OS
A375 p53 wt
A375 p53 -/-
s9.6
DAPI s9.6
Cytoplasmic s9.6 Intensity (a.u.)
3'
TGCCCAGGCTTGCTT
ACGGGTCCGAACGAA
GGTTACCCTCAAAGGAAAGCC
ATGAAGCTTAGTTTGGCTGG
AAATGGTGCTGGGAAAACTG
GTTTTGGACATGAAGTCCTTGC
% Input (IP with s9.6)
RPL13A
ZNF544
L1-ORF1
L1-ORF2
ns
DAPI RNH
% Input (IP with RNH-GFP)
Input
DRIP-seq
GRO-seq
chr7:
196,696,600
196,697,580
196,698,600
196,699,870
Repeating Elements by RepeatMasker
LINE

Figure 2

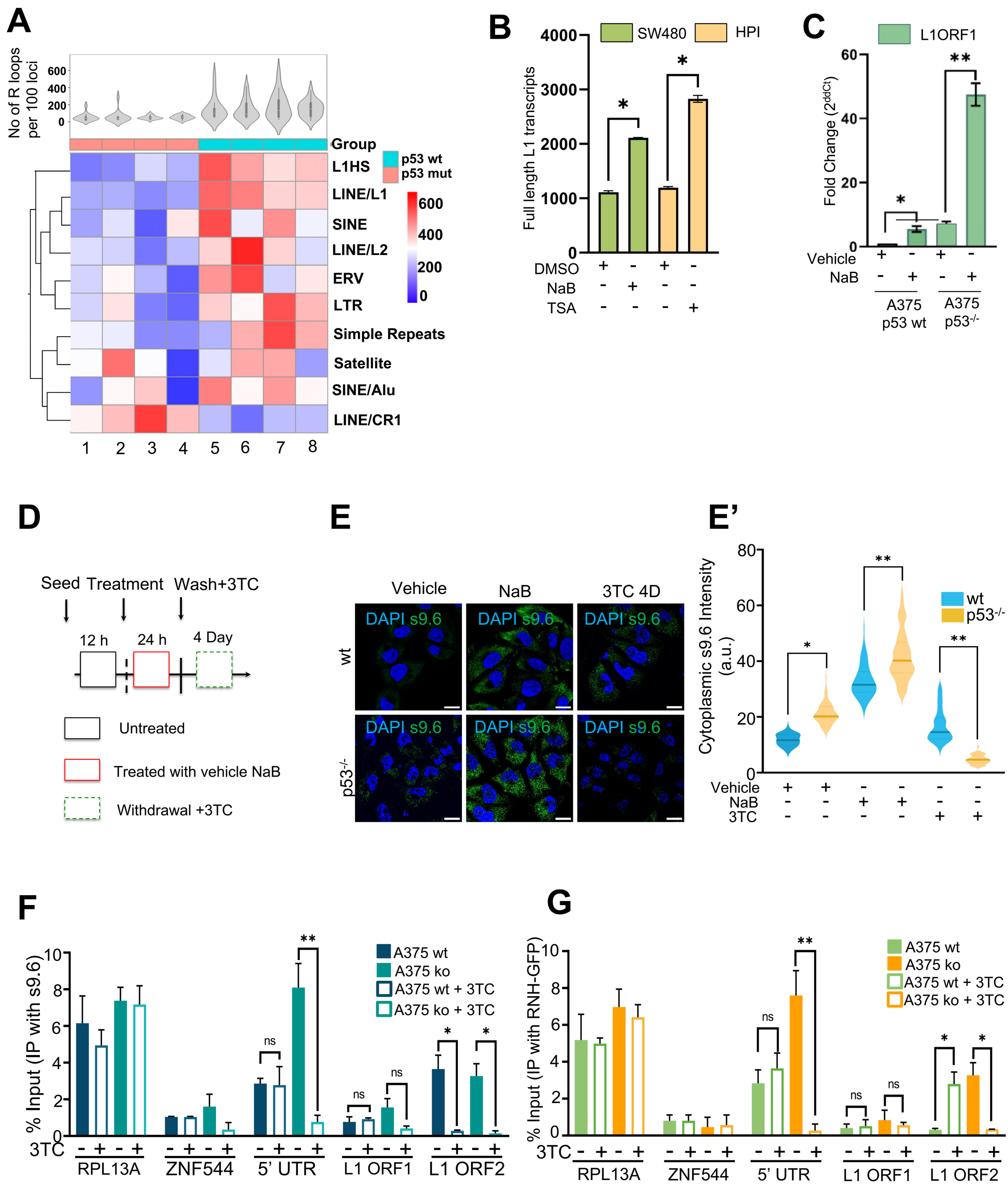
A
No of R loops per 100 loci
Group
p53 wt
p53 mut
L1HS
LINE/L1
SINE
LINE/L2
ERV
LTR
Simple Repeats
Satellite
SINE/Alu
LINE/CR1
1 2 3 4 5 6 7 8
B
SW480
HPI
Full length L1 transcripts
DMSO
NaB
TSA
C
L1ORF1
Fold Change (2ddCt)
Vehicle
NaB
A375 p53 wt
A375 p53-/-
D
Seed Treatment Wash+3TC
12 h
24 h
4 Day
Untreated
Treated with vehicle NaB
Withdrawal +3TC
E
Vehicle
NaB
3TC 4D
DAPI s9.6
wt
p53-/-
E'
Cytoplasmic s9.6 Intensity (a.u.)
wt
p53-/-
Vehicle
NaB
3TC
F
% Input (IP with s9.6)
A375 wt
A375 ko
A375 wt + 3TC
A375 ko + 3TC
3TC
RPL13A
ZNF544
5' UTR
L1 ORF1
L1 ORF2
G
% Input (IP with RNH-GFP)
A375 wt
A375 ko
A375 wt + 3TC
A375 ko + 3TC
3TC
RPL13A
ZNF544
5' UTR
L1 ORF1
L1 ORF2

Figure 3

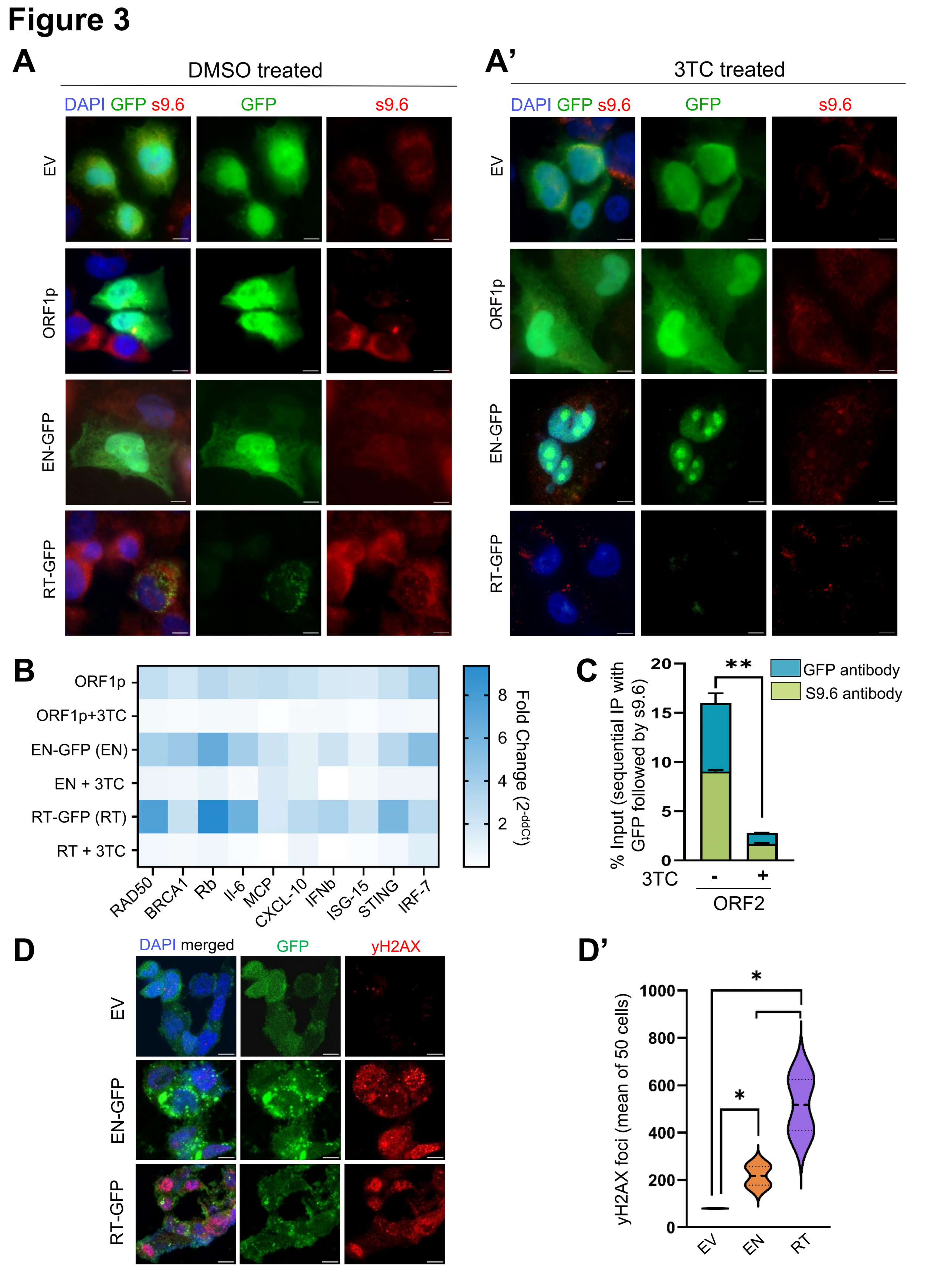
A
DMSO treated
DAPI GFP s9.6
GFP
s9.6
EV
ORF1p
EN-GFP
RT-GFP
A'
3TC treated
DAPI GFP s9.6
GFP
s9.6
EV
ORF1p
EN-GFP
RT-GFP
B
ORF1p
ORF1p+3TC
EN-GFP (EN)
EN + 3TC
RT-GFP (RT)
RT + 3TC
RAD50
BRCA1
Rb
Il-6
MCP
CXCL-10
IFNb
ISG-15
STING
IRF-7
Fold Change (2-ddCt)
8
6
4
2
C
% Input (sequential IP with GFP followed by s9.6)
20
15
10
5
0
**
GFP antibody
S9.6 antibody
3TC
-
+
ORF2
D
DAPI merged
GFP
yH2AX
EV
EN-GFP
RT-GFP
D'
yH2AX foci (mean of 50 cells)
1000
800
600
400
200
0
*
*
EV
EN
RT

Figure 4

A

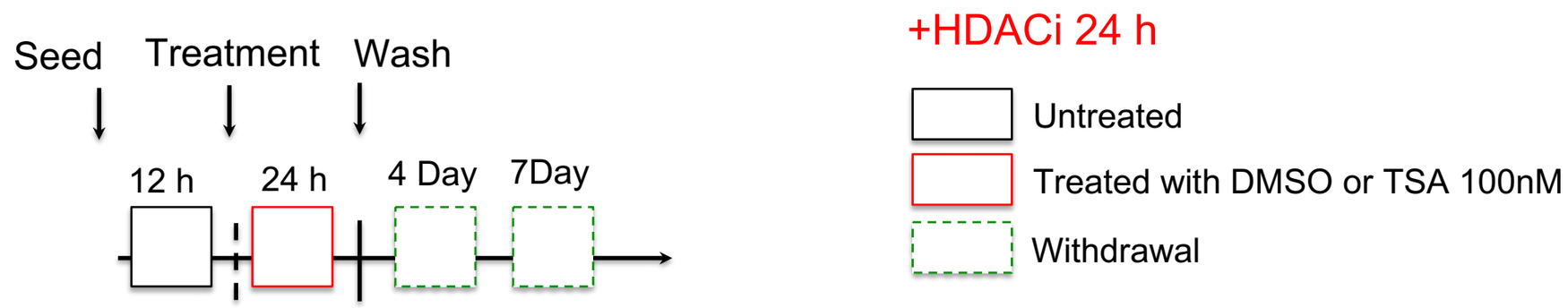

B

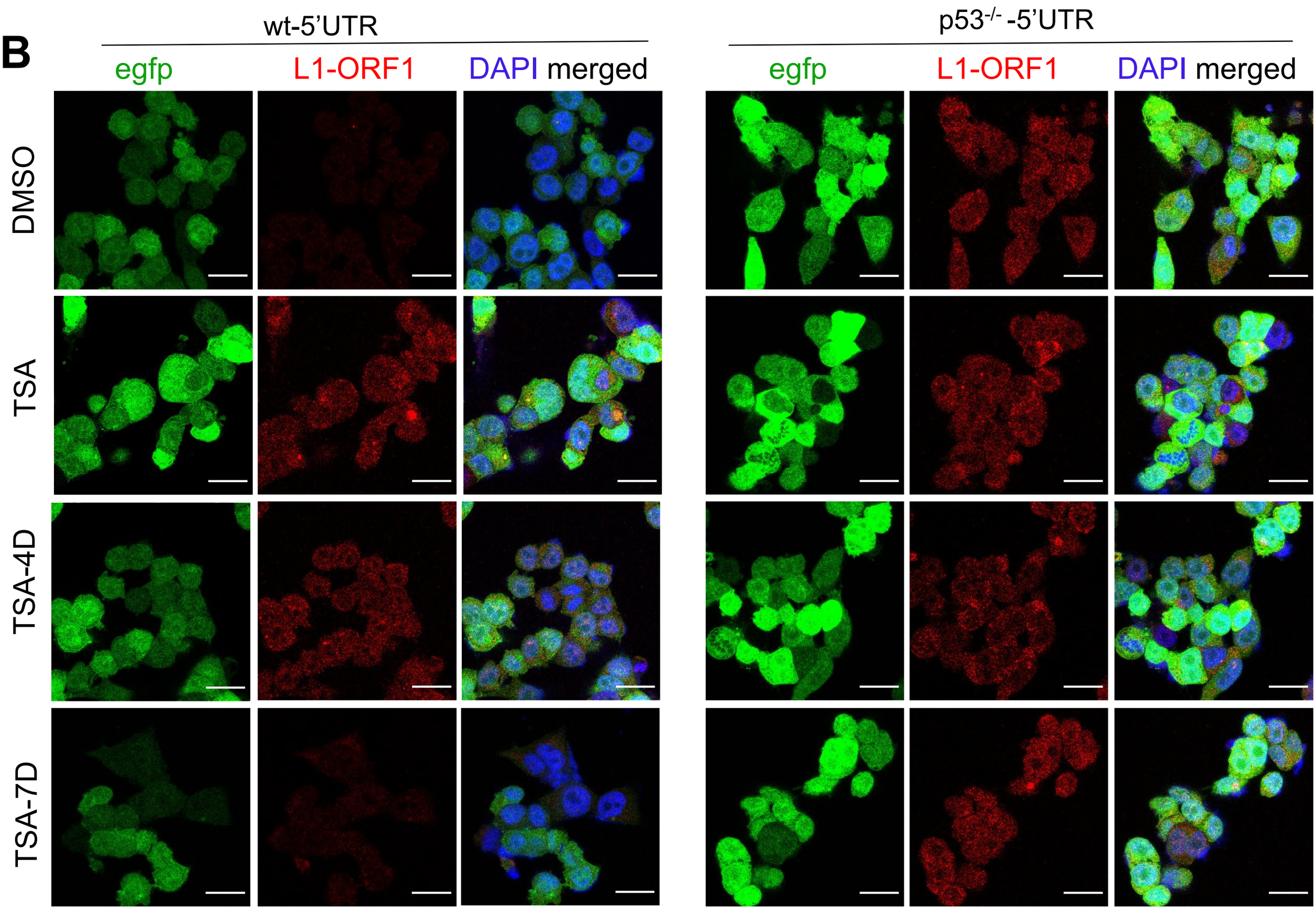

C

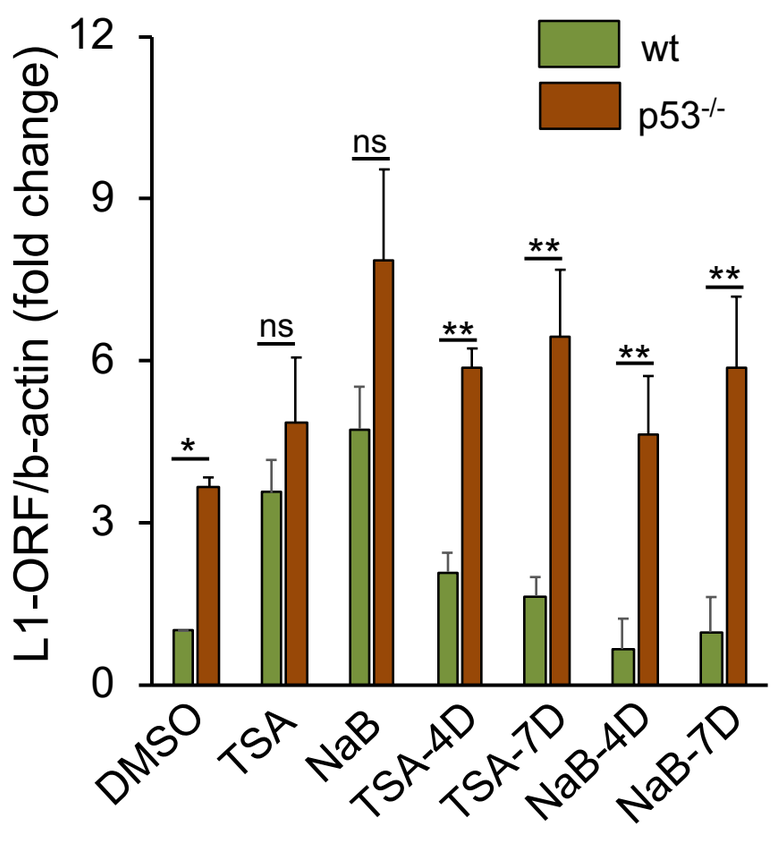

D

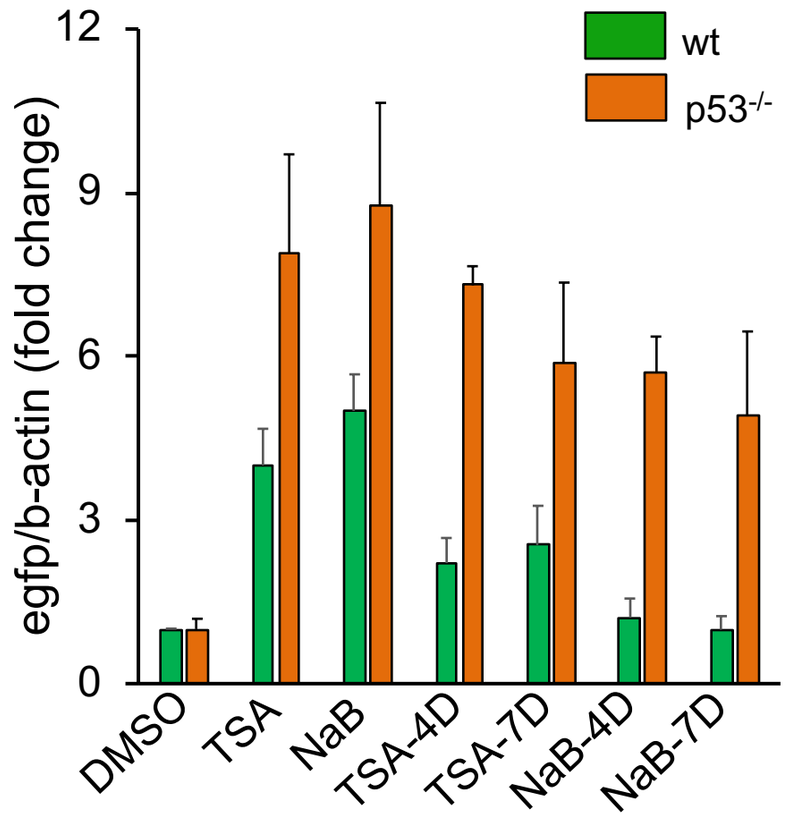

E

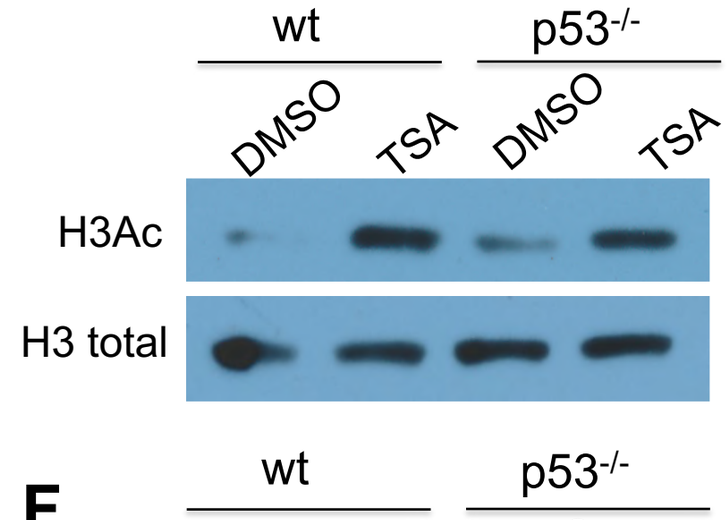

F

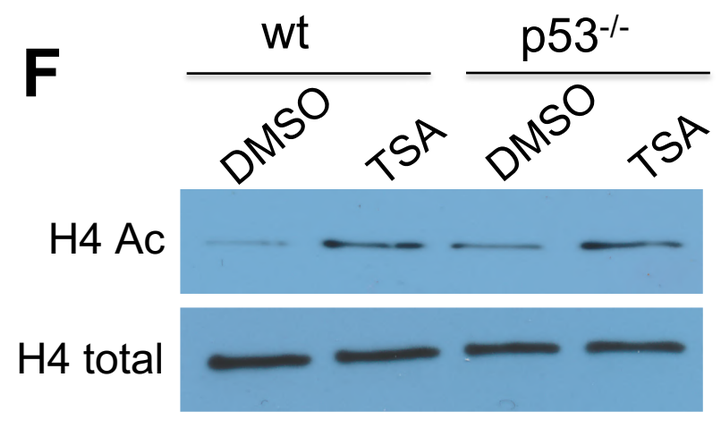

Figure 5

A

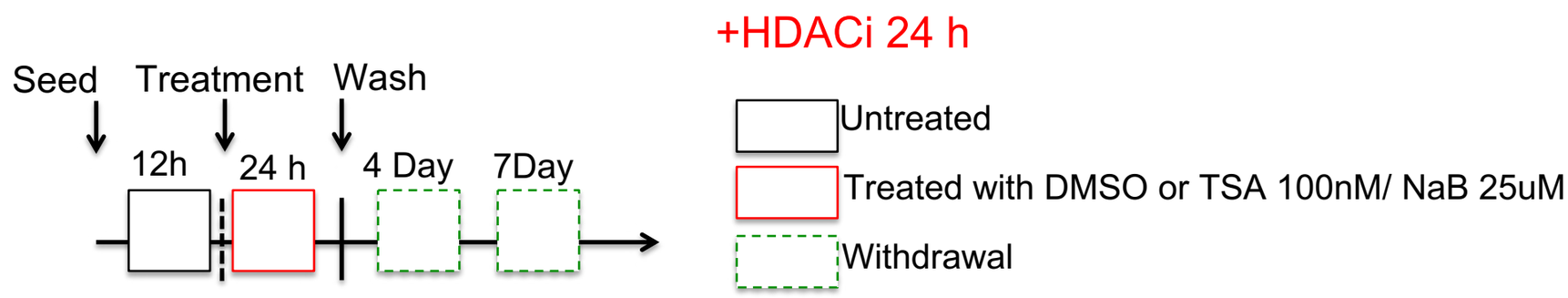

B

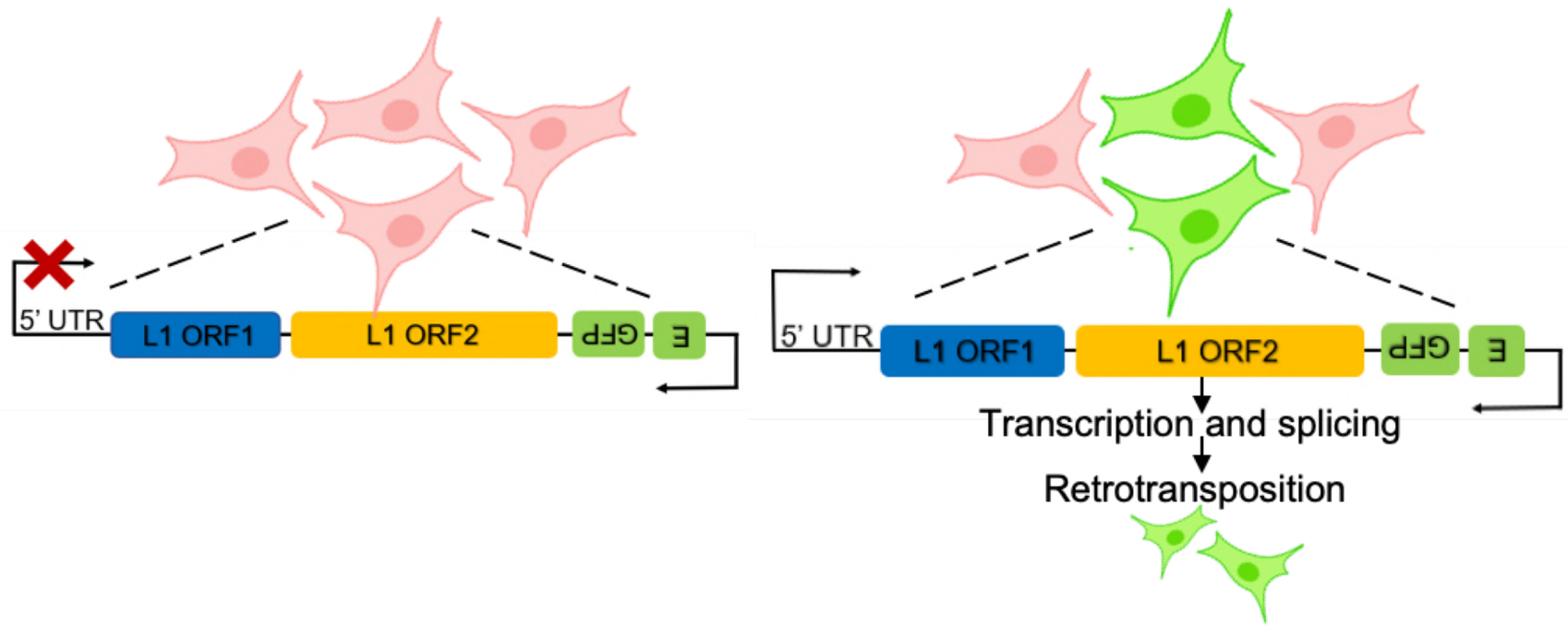

C

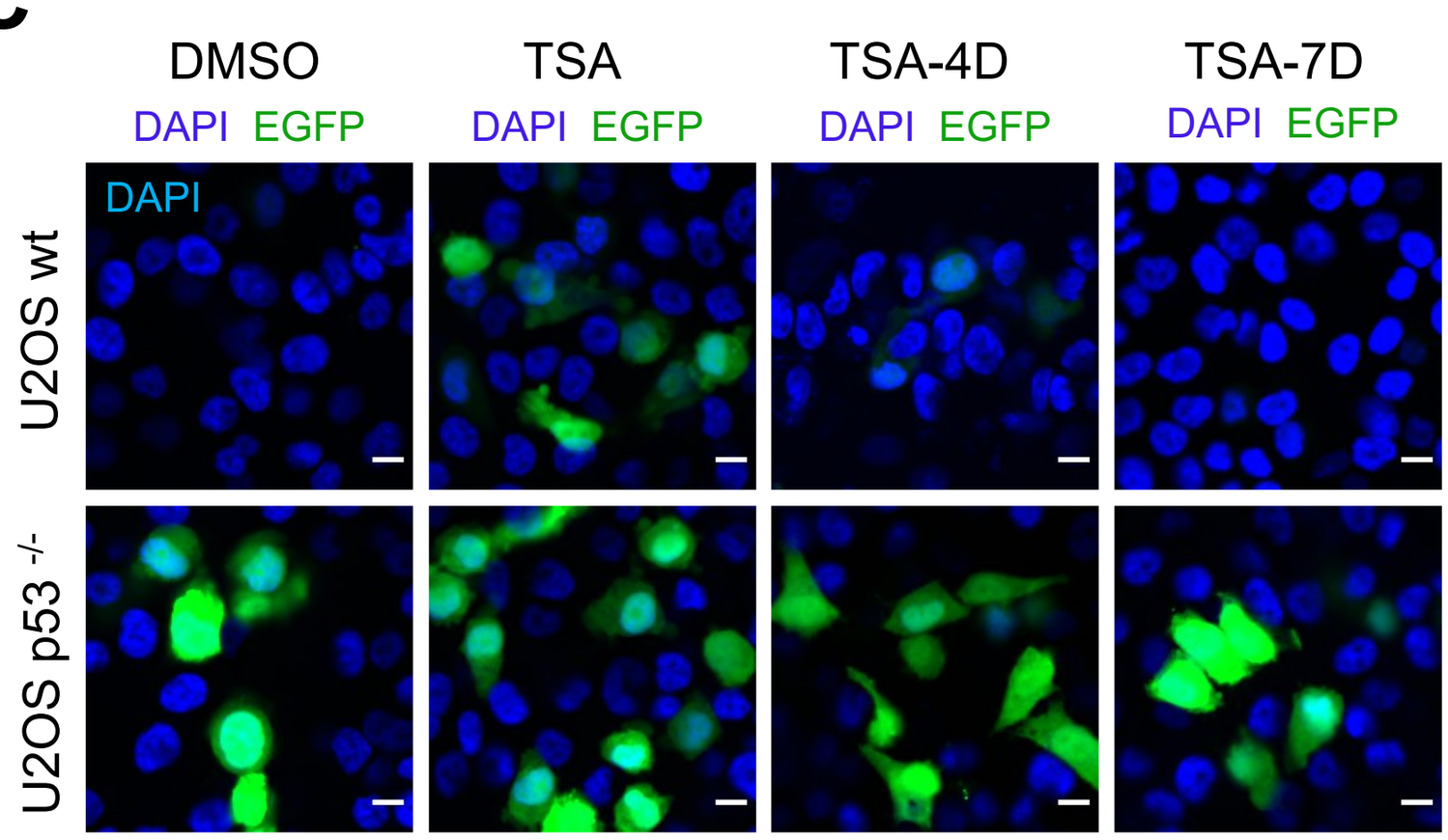

C'

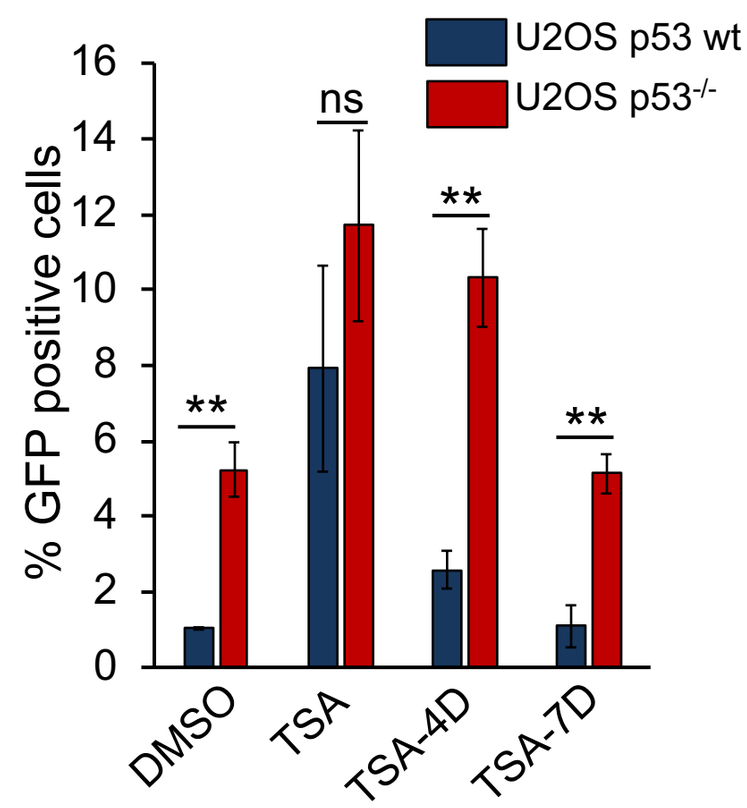

D

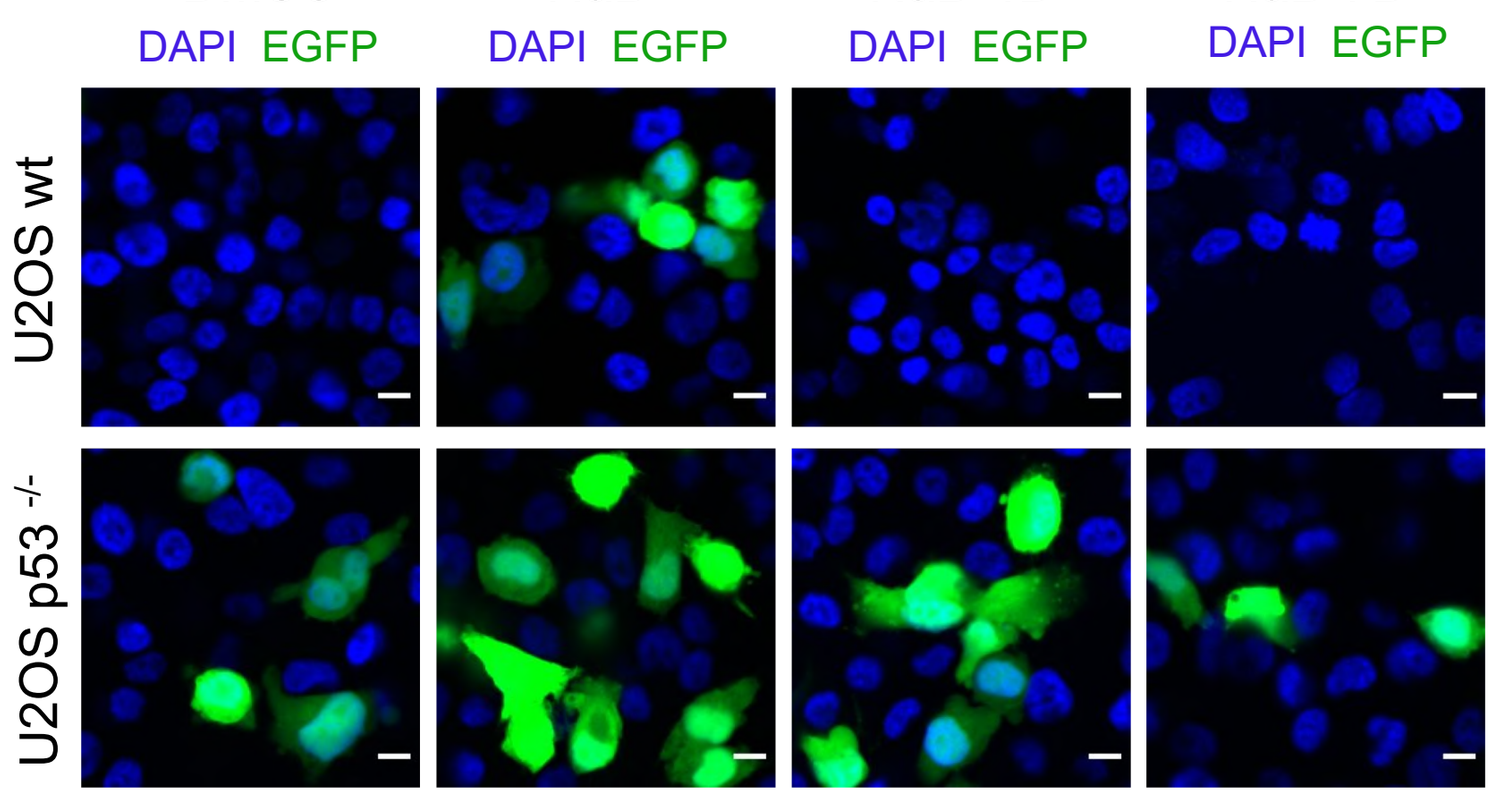

D'

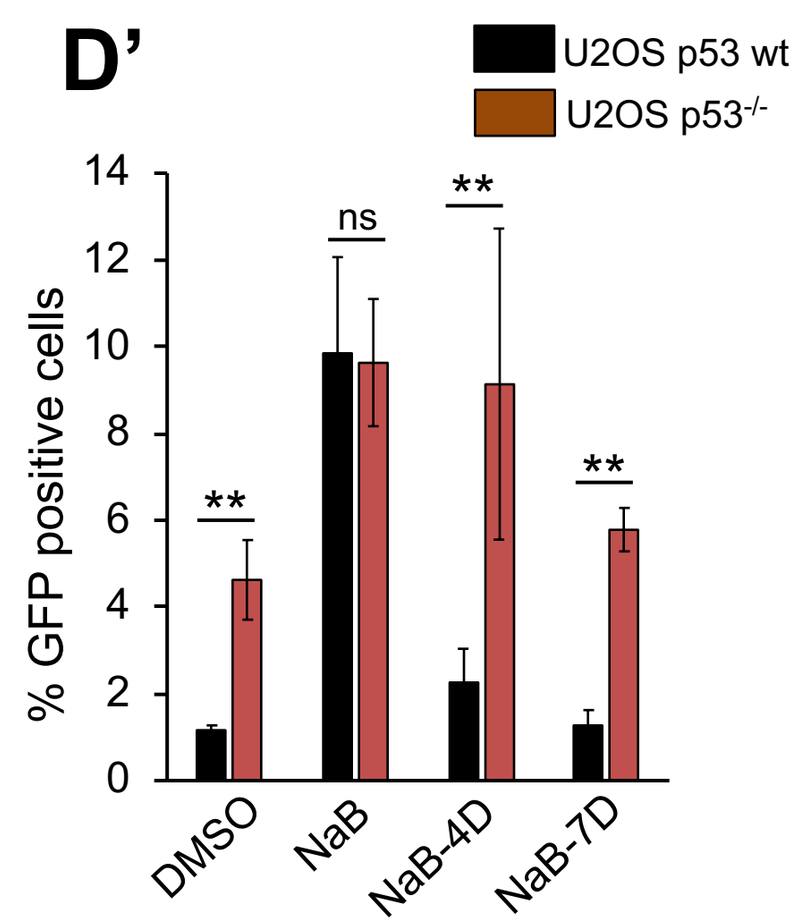

Figure 5

A

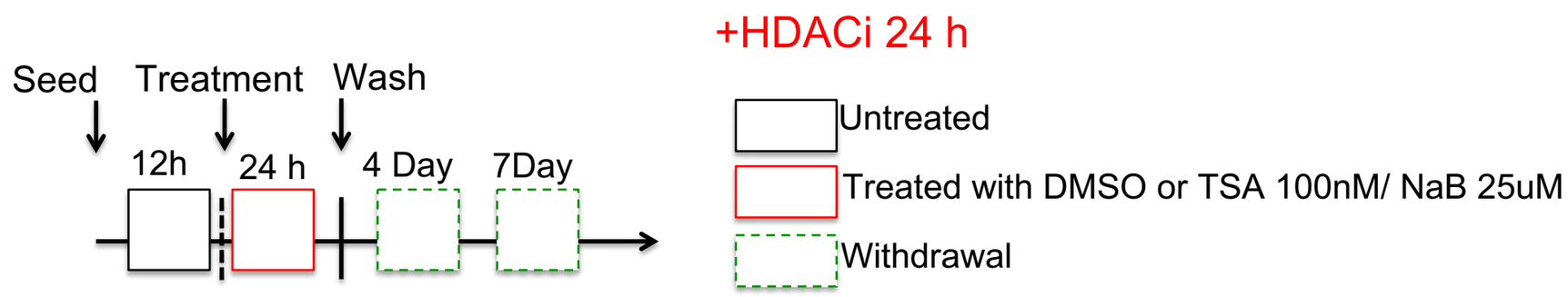

B

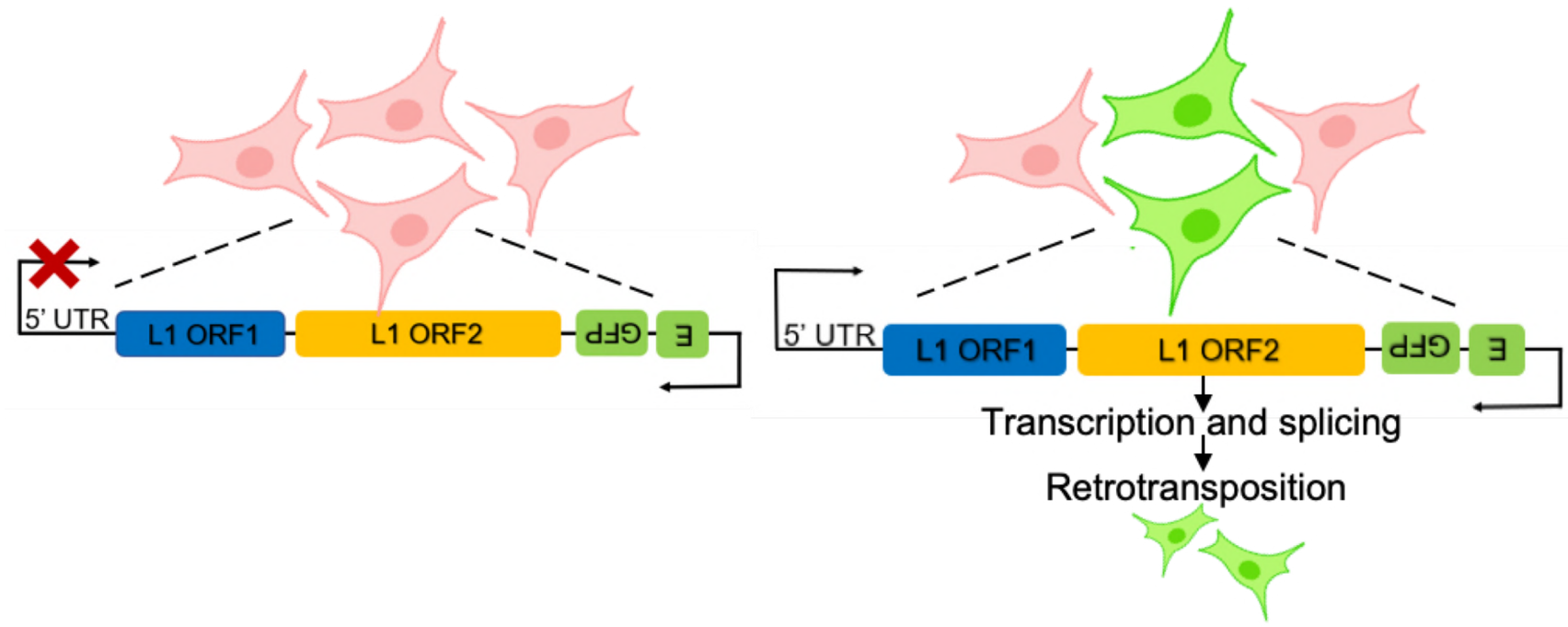

C

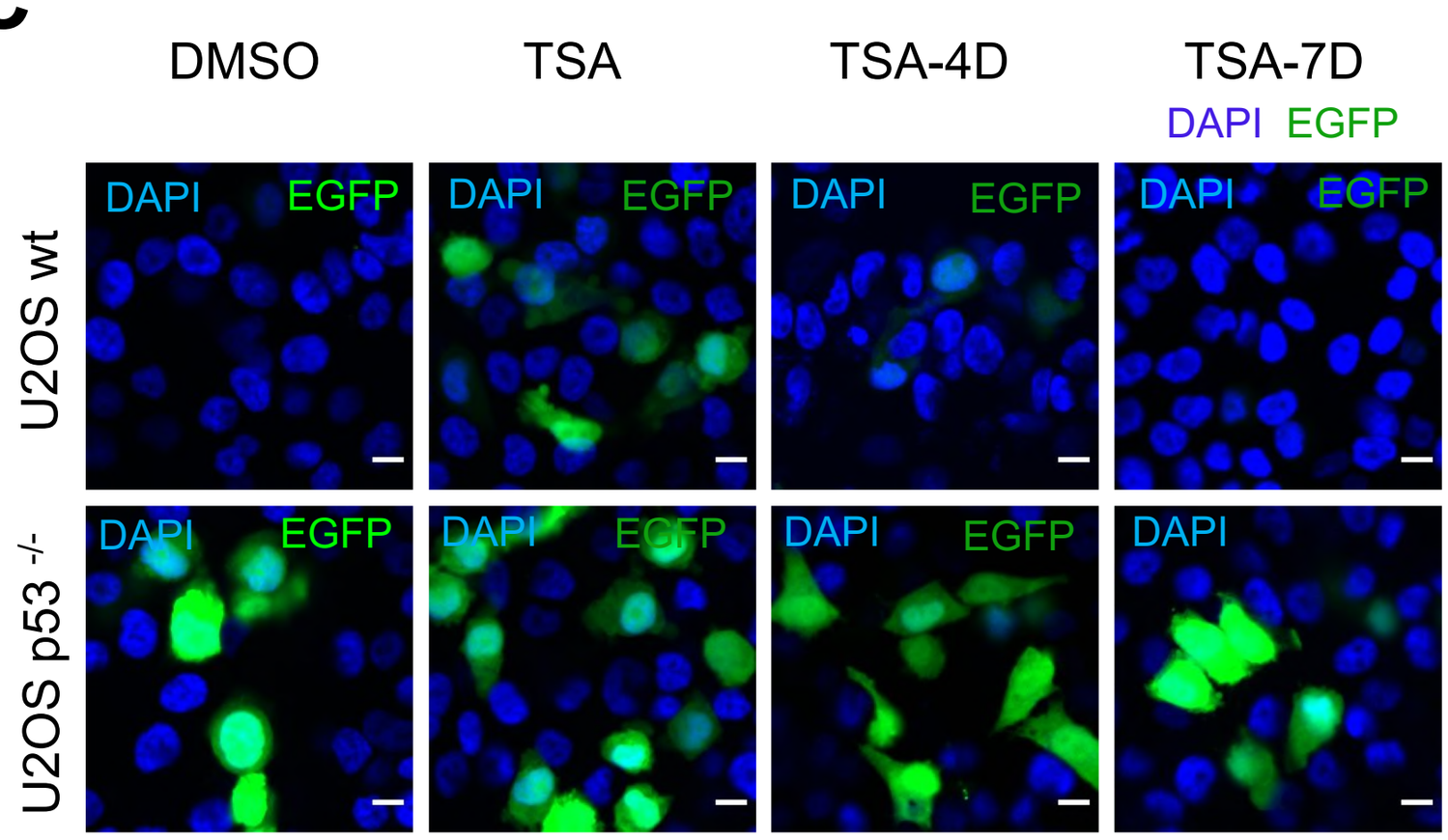

C'

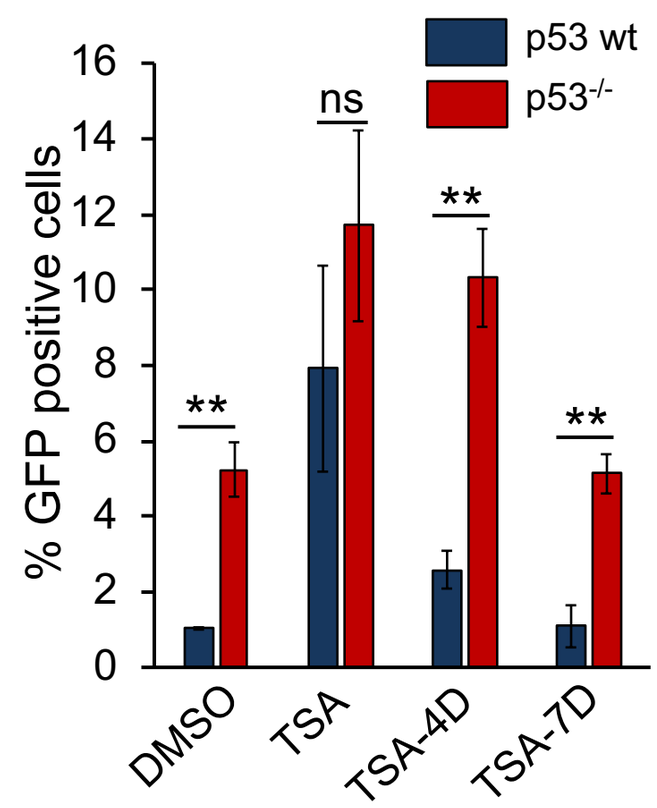

D

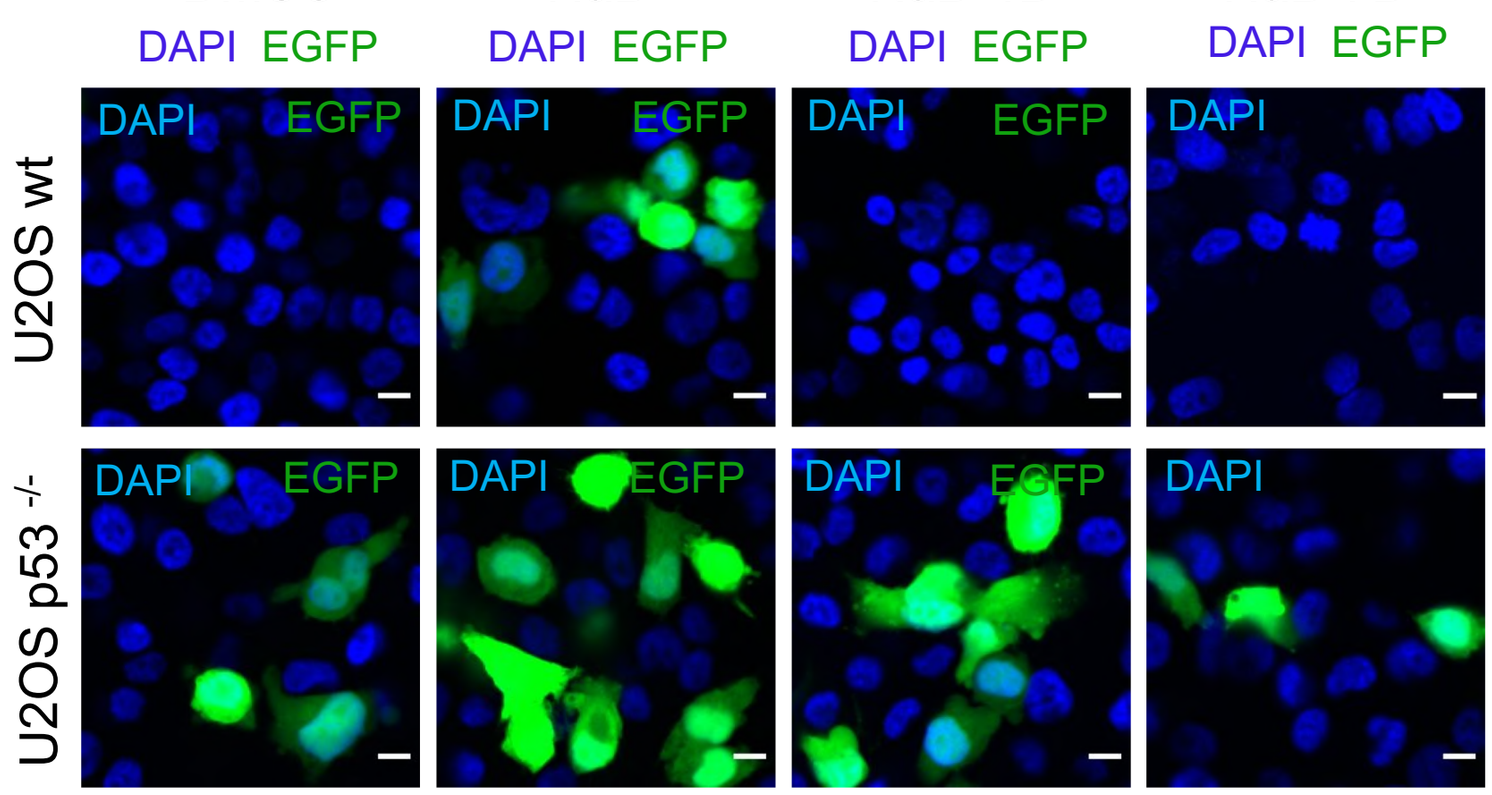

D'

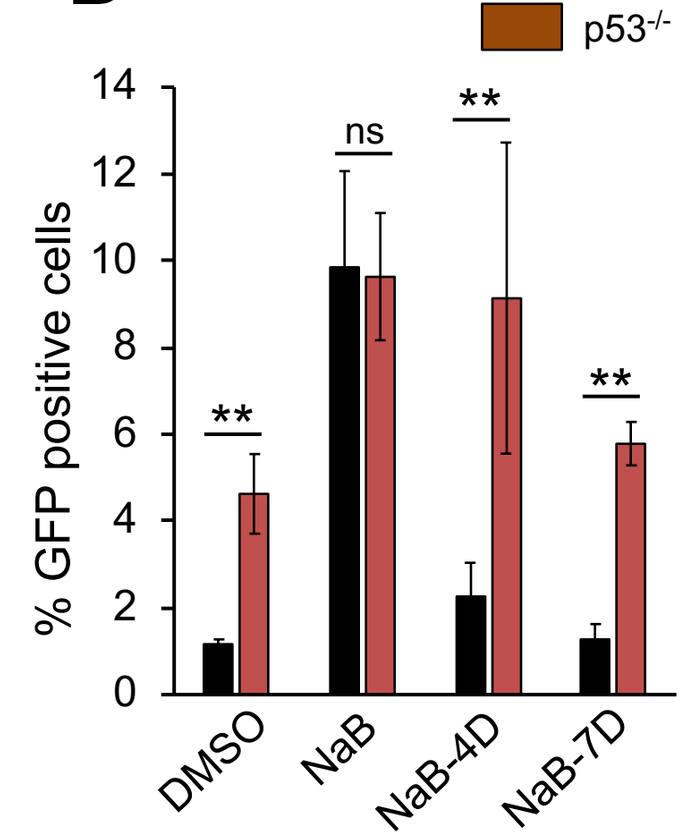

Figure 6

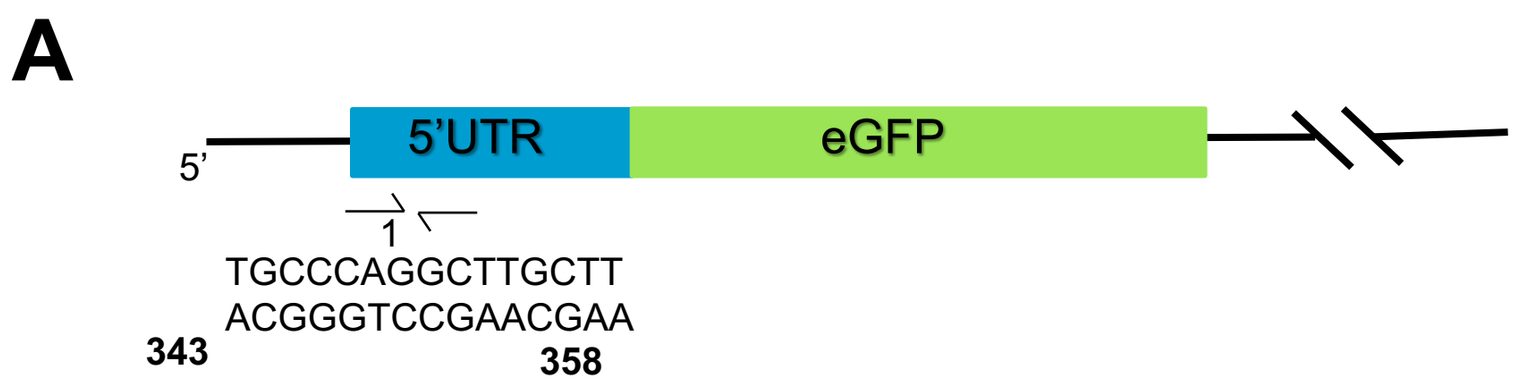
A
5'
5'UTR
eGFP
1
TGCCCAGGCTTGCTT
ACGGGTCCGAACGAA
343
358

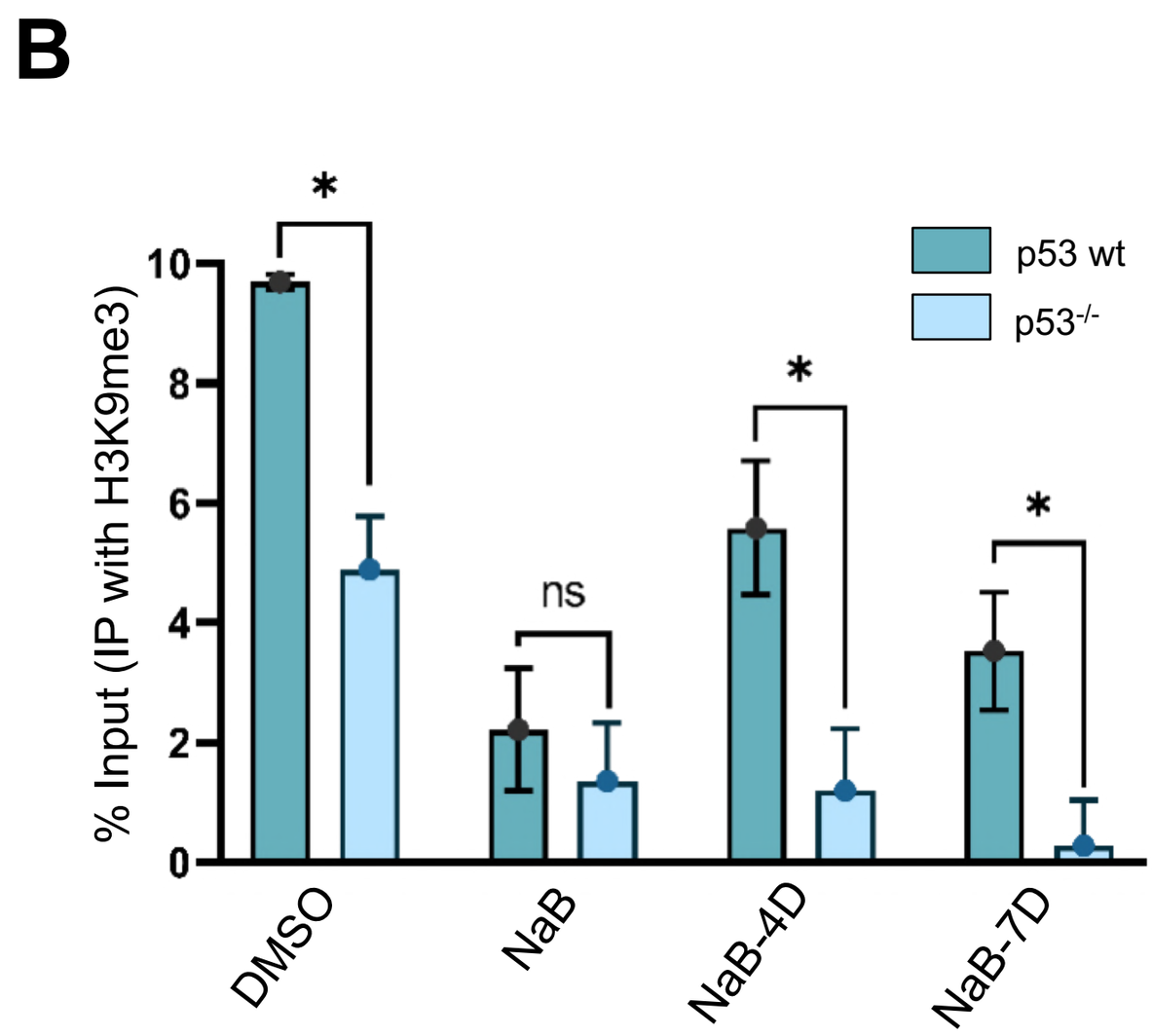
B
% Input (IP with H3K9me3)
p53 wt
p53-/-
*
ns
*
*
DMSO
NaB
NaB-4D
NaB-7D

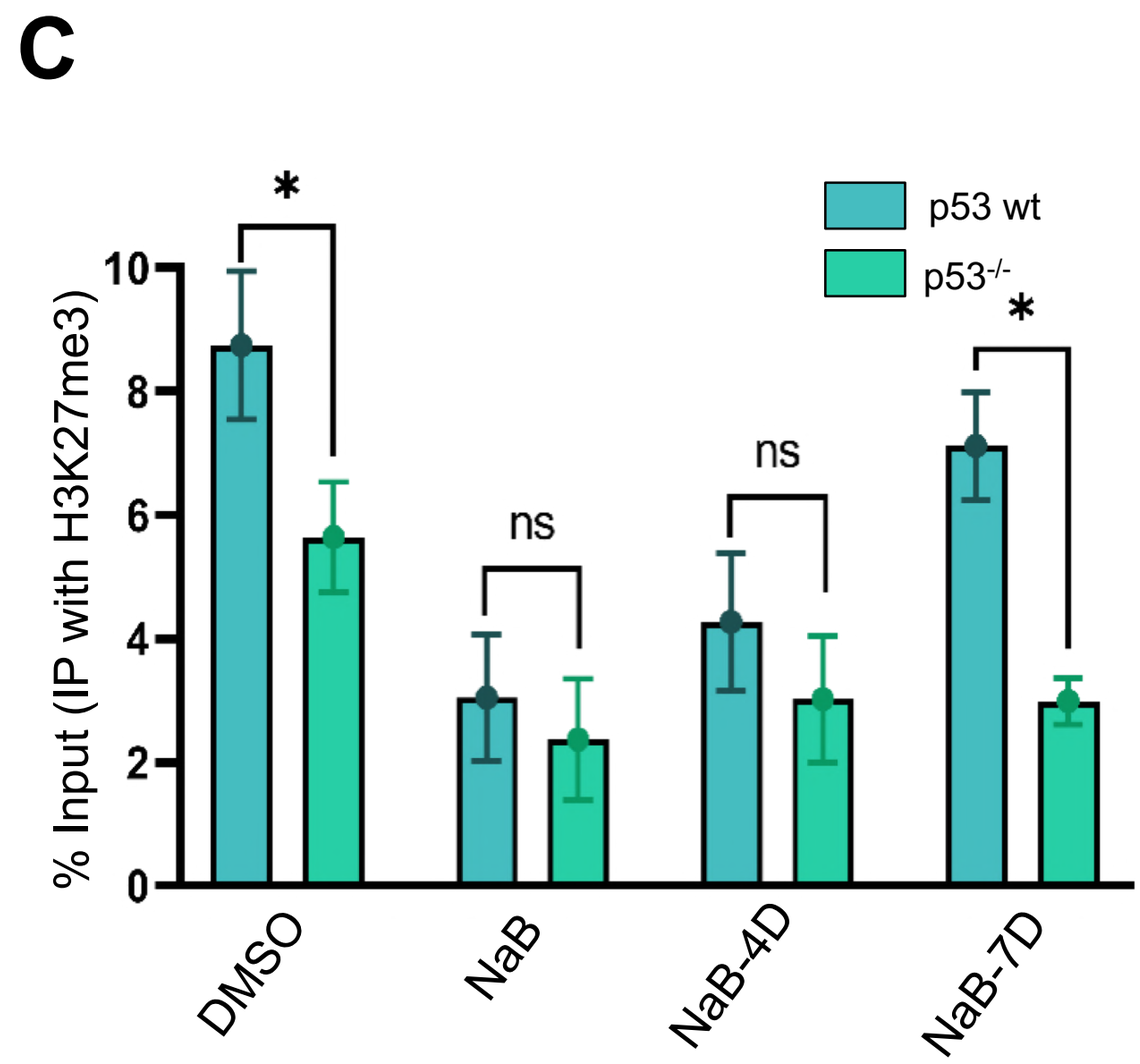
C
% Input (IP with H3K27me3)
p53 wt
p53-/-
*
ns
ns
*
DMSO
NaB
NaB-4D
NaB-7D

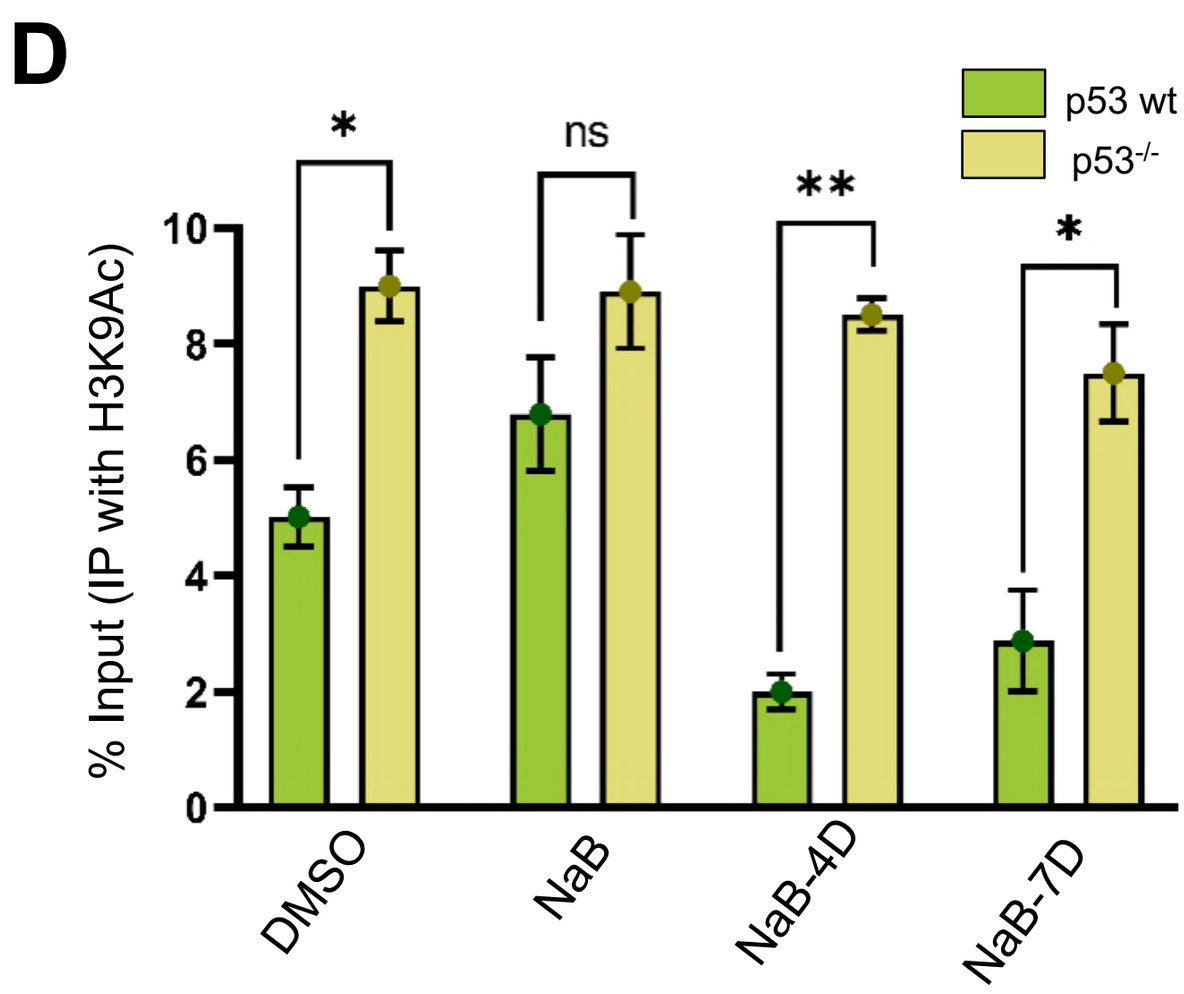
D
% Input (IP with H3K9Ac)
p53 wt
p53-/-
*
ns
**
*
DMSO
NaB
NaB-4D
NaB-7D

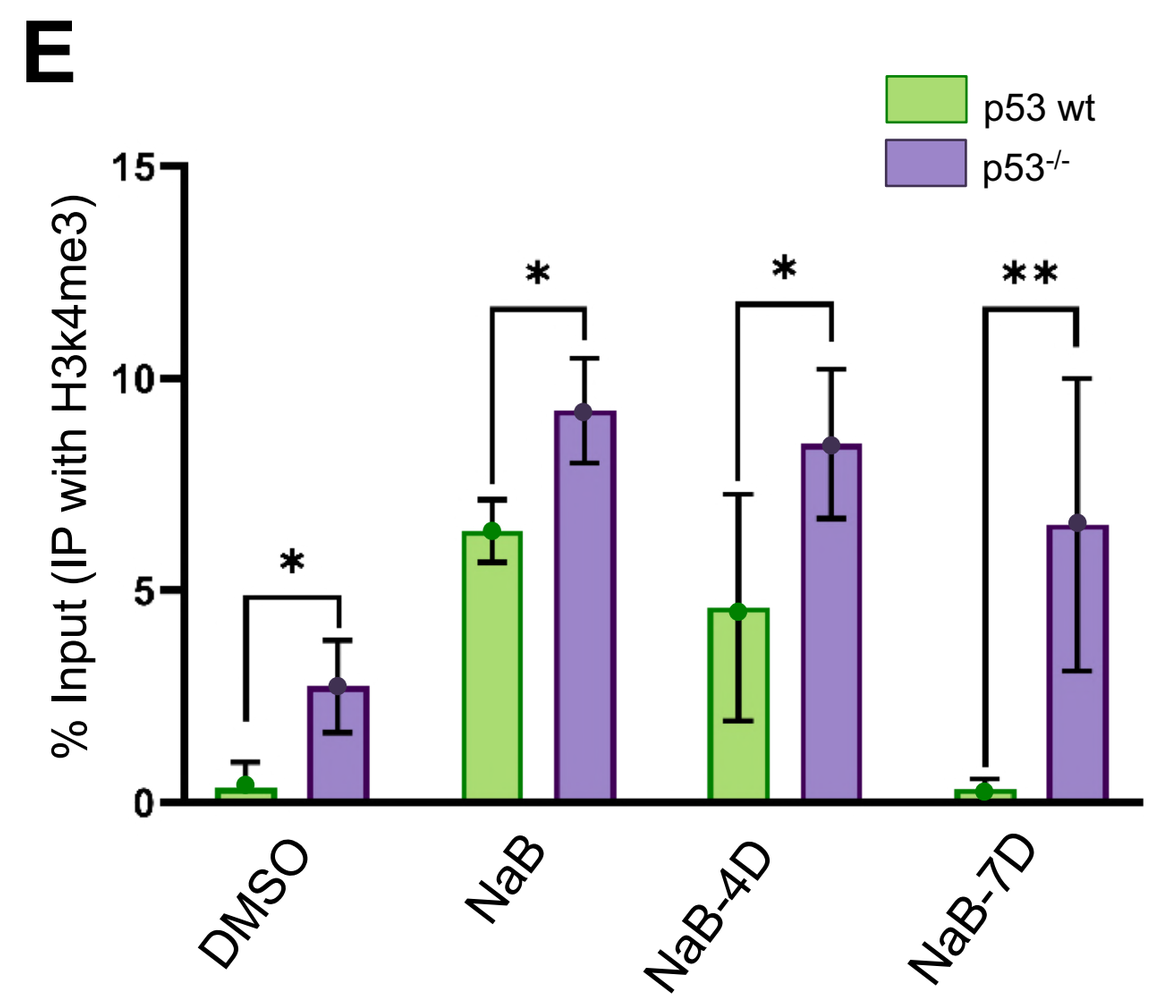
E
% Input (IP with H3k4me3)
p53 wt
p53-/-
*
*
*
**
DMSO
NaB
NaB-4D
NaB-7D

Figure 7

A

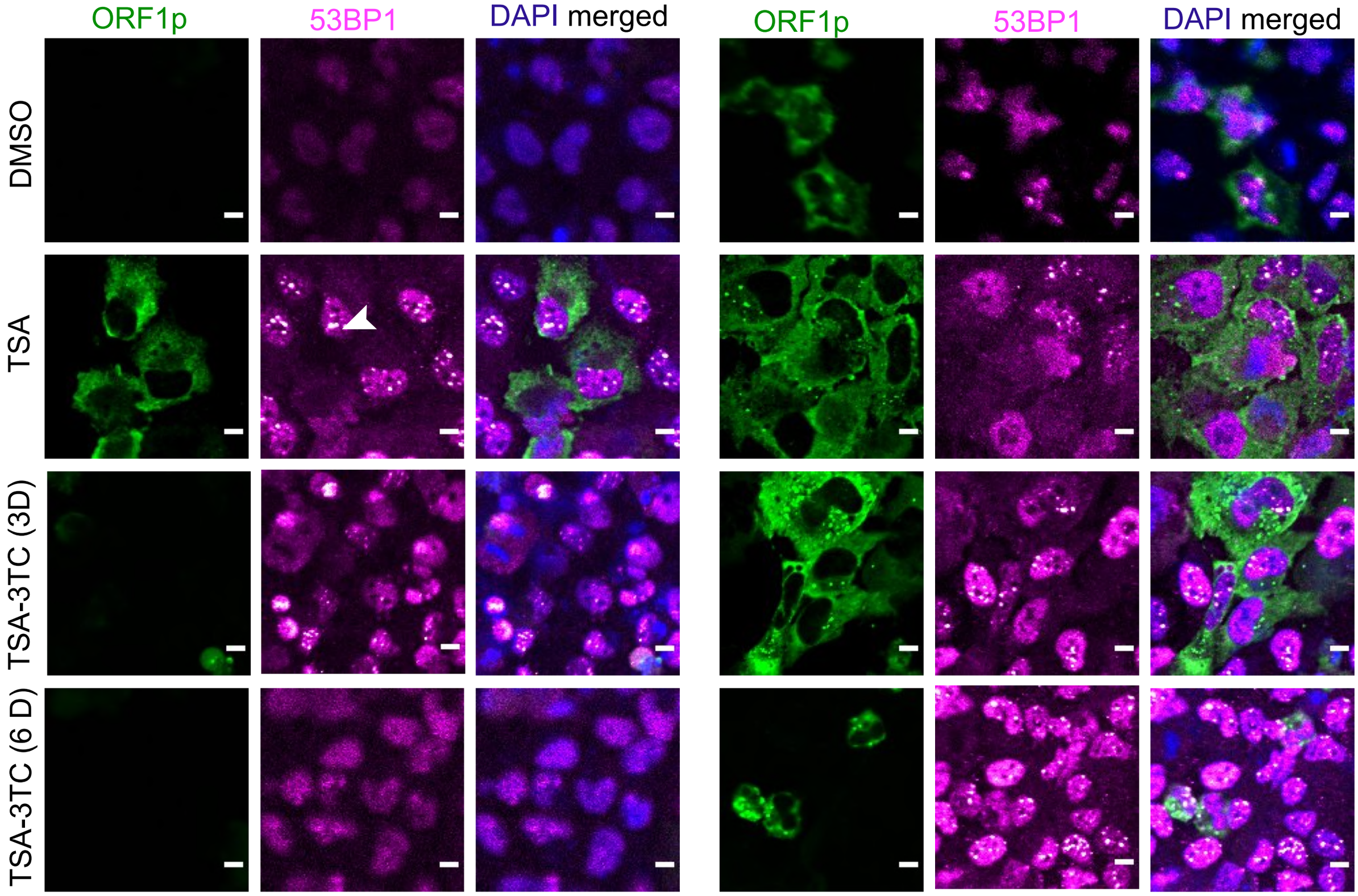
ORF1p
53BP1
DAPI merged
ORF1p
53BP1
DAPI merged
DMSO
TSA
TSA-3TC (3D)
TSA-3TC (6 D)

A'

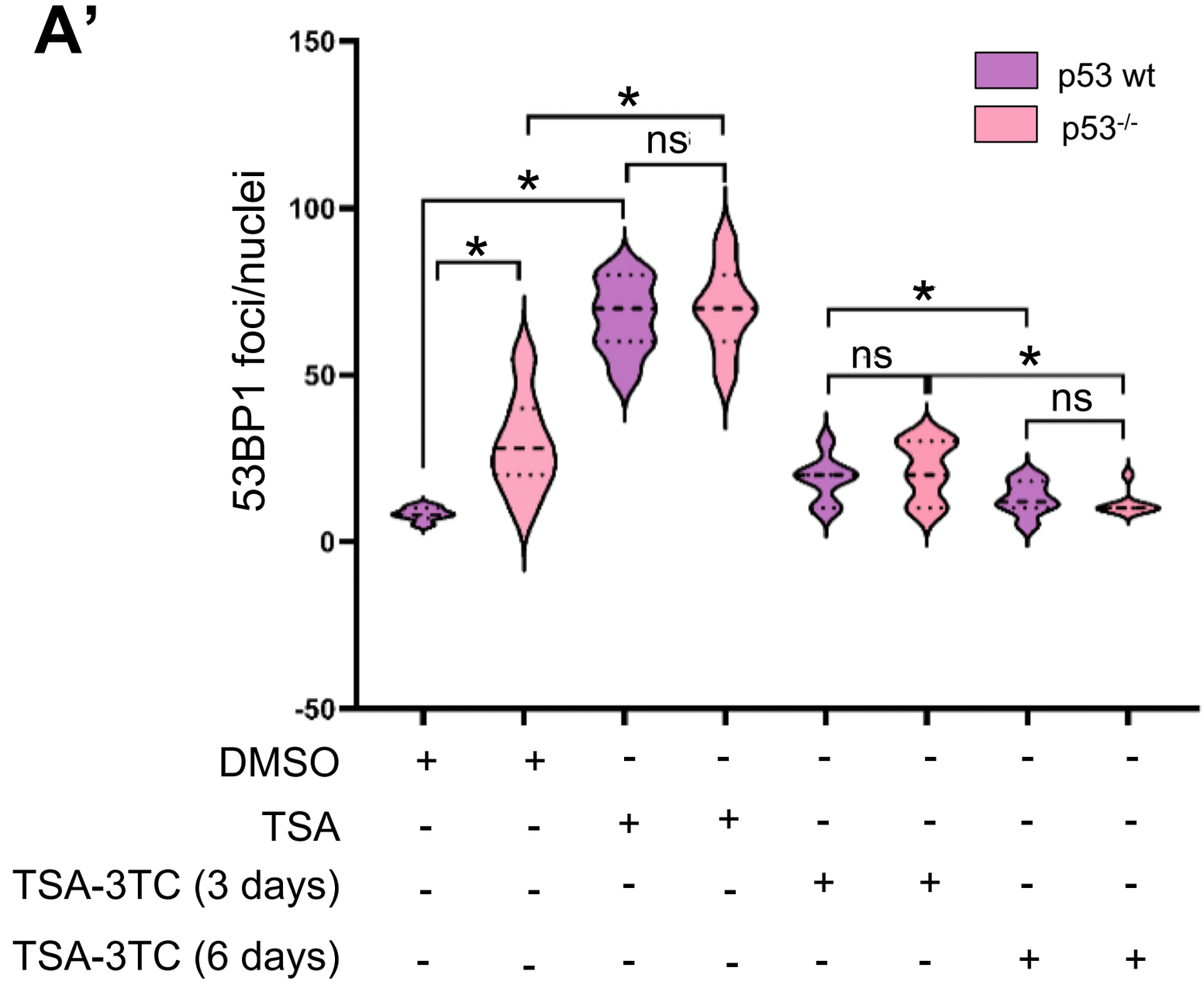
53BP1 foci/nuclei
150
100
50
0
-50
p53 wt
p53-/-
*
ns
*
*
*
ns
*
ns
DMSO + + - - - - - -
TSA - - + + - - - -
TSA-3TC (3 days) - - - - + + - -
TSA-3TC (6 days) - - - - - - + +

Figure 6

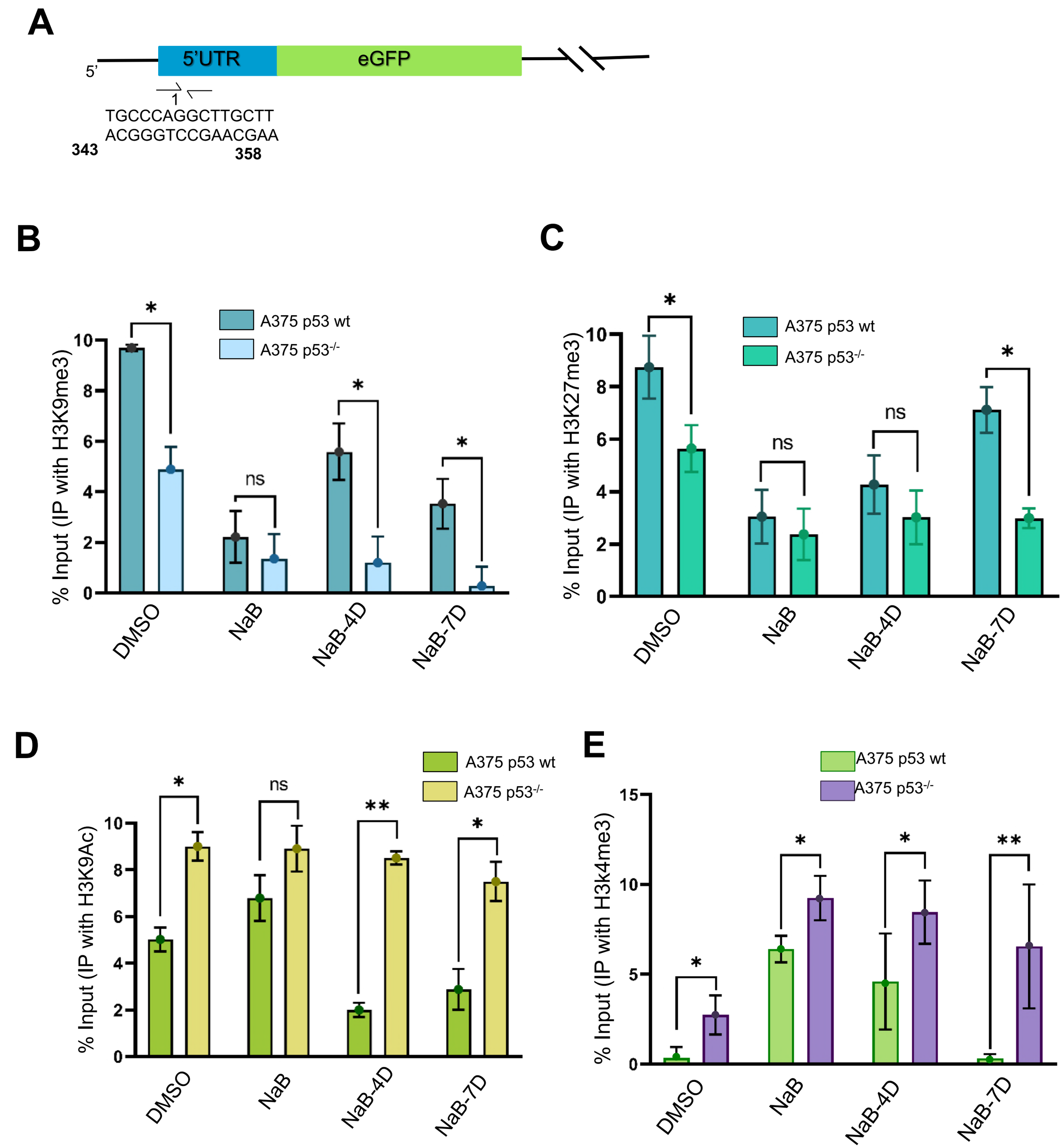
A
5'
5'UTR
eGFP
1
TGCCCAGGCTTGCTT
ACGGGTCCGAACGAA
343
358
B
A375 p53 wt
A375 p53-/-
% Input (IP with H3K9me3)
DMSO
NaB
NaB-4D
NaB-7D
ns
C
A375 p53 wt
A375 p53-/-
% Input (IP with H3K27me3)
DMSO
NaB
NaB-4D
NaB-7D
ns
D
A375 p53 wt
A375 p53-/-
% Input (IP with H3K9Ac)
DMSO
NaB
NaB-4D
NaB-7D
ns
E
A375 p53 wt
A375 p53-/-
% Input (IP with H3k4me3)
DMSO
NaB
NaB-4D
NaB-7D